

Prior Knowledge or Search? A Study of LLM Agents in Hardware-Aware Code Optimization

Dmitry Redko*

Applied AI Institute
dmitryredko444@gmail.com

Albert Fazlyev*

AI Talent Hub, ITMO University
albert.fz@yandex.ru

Konstantin Sozykin*

Applied AI Institute
k.sozykin@applied-ai.ru

Maria Ivanova

YSDA, Applied AI Institute
ivanova.m.pe@gmail.com

Evgeny Burnaev

Applied AI Institute
e.burnaev@applied-ai.ru

Egor Shvetsov

Applied AI Institute
e.shvetsov@applied-ai.ru

*Authors contributed equally to this work.

Abstract

LLM discovery and optimization systems are increasingly applied across domains, implementing a common propose-evaluate-revise loop. Such optimization or discovery progresses via context conditioning on received feedback from an environment. However, as modern LLM agents are increasingly complex in their structure, it is difficult to evaluate which components contribute the most, and when and how this exploration may fail. We answer these questions through three controlled experiments. Our findings: (1) In pure black-box optimization, LLMs act as greedy optimizers. (2) In zero-shot kernel generation, providing explicit input-size information has no measurable effect, models converge to the same kernel parameters regardless of size or temperature, as though the size instruction were invisible. Moreover, when tasked to perform kernel optimization for uncommon kernel sizes, performance sharply degrades regardless of the language used. (3) In feedback-loop kernel optimization, CUDA improves monotonically under iterative feedback, while TVM IR actively degrades, which demonstrates that kernel optimization degrades when models operate with low-density language. Our results conclude that LLMs in code optimization tasks highly depend on pretrained priors rather than provided feedback or agentic structure.

1 Introduction

Large language models are increasingly deployed as autonomous discovery systems that propose candidate solutions, observe evaluative feedback, and iterate toward novel results. Recent successes span extremal combinatorics (Romera-Paredes et al., 2024), matrix multiplication (Novikov et al., 2025), scientific equation discovery (Shojaee et al., 2025), chemistry (Yang et al., 2025), and GPU kernel optimization (Ouyang et al., 2025; Lange et al., 2025) all sharing the same high level structure: *propose* \rightarrow *evaluate* \rightarrow *revise* loop.

This pattern is structurally identical to black-box optimization (Shahriari et al., 2015), but with a key difference: a surrogate model updates a posterior over the objective landscape while the LLM encodes its prior in frozen weights and adapts solely through context conditioning. Therefore, LLMs would excel when the prior is dense over the target solution space but degrade as it drifts from what the model has seen, while

BBO is task-adaptive but becomes intractable as the search space grows. **This raises a precise question: *How and where exactly does LLM-based discovery break down?*** We investigate this in two controlled settings. In pure black-box optimization over unknown functions, where the prior is effectively absent, we find that LLMs follow greedy, refinement-like trajectories rather than exploring. In low-level kernel optimization, we control prior density along two axes: (1) Representation language, contrasting CUDA, richly present in pretraining data, with TVM intermediate representation, which is found 100 times less in pretraining data (Kocetkov et al., 2023). (2) Solution space familiarity, contrasting standard kernel sizes likely seen during pretraining with small atypical sizes that are rarely encountered.

We summarize our findings and contributions as follows:

- Empirical evidence that LLMs perform greedy optimization and require orchestrated exploration to escape it.** LLMs act as greedy optimizers in pure BBO settings, losing to BBO algorithms on tasks that require genuine exploration. Wrapping the LLM in an agentic system with explicit exploration orchestration recovers this gap and outperforms either approach in isolation.
- Prior collapse in kernel generation: LLMs produce size-agnostic solutions regardless of explicitly specified input dimensions.** Zero-shot generation produces kernels with generic parameters regardless of stated tensor dimensions or sampling temperature. This directly causes domain-shift degradation: on small input sizes the fraction of accelerated kernels drops from 59% to 31%, while the BBO like approach (TVM MetaSchedule) not only does not degrade but actually improves from 41% to 69%.
- Weak language priors degrade iterative feedback-loop exploration.** The quality of the LLM prior over the target language determines whether iterative optimization converges or deteriorates: correctly compiled kernels increase monotonically for CUDA but decrease at each step for TVM IR, where the prior is too weak to support the feedback loop.

Practical implications: Modern agentic pipelines combine context manipulation, iterative feedback, population-based evolution, and randomized search in ways that make it difficult to attribute performance to any single factor. By working in controlled, minimal settings we isolate these factors and expose failure modes fundamental to any LLM-based discovery system, with direct implications for the design of LLM agents.

Paper roadmap: Section 2 frames LLM discovery as a form of black-box optimization with a frozen, context-conditioned prior. Section 3 tests this view in pure BBO, where no strong code prior is available, and shows that LLMs behave as greedy local refiners. Section 4 then moves to kernel optimization, where we vary prior alignment through input shape, program representation, and feedback architecture. Finally, Section 5 interprets these results and discusses when LLM agents should be paired with explicit search or retrieval rather than used as standalone optimizers. Related work and additional experimental details and results are deferred to the appendix.

2 A Formal View of LLM Agents vs. BBO Discovery

We compare LLM agents and black-box optimization (BBO) within the same outer optimization loop: both repeatedly propose a candidate, evaluate it, and use the observed feedback to guide the next proposal. The key difference is what state is allowed to adapt after each evaluation.

For a task instance τ , let $x \in \mathcal{X}_\tau$ denote a candidate and $y = F_\tau(x)$ its scalar evaluation metric. After k evaluations, $\mathcal{D}_k = \{(x_i, y_i)\}_{i=1}^k$. For LLM agents we additionally define a context $c_k \in \mathcal{C}$ comprising the task description, previous candidates and scores, compiler errors, and any other tool feedback visible at step k . Both LLM agents and BBO share the same outer loop with proposal distribution q_k :

$$\begin{aligned} x_{k+1} &\sim q_k(\cdot), \\ y_{k+1} &= F_\tau(x_{k+1}), \\ \mathcal{D}_{k+1} &= \mathcal{D}_k \cup \{(x_{k+1}, y_{k+1})\}. \end{aligned} \quad (1)$$

Optimization succeeds when q_k concentrates on high-reward regions of \mathcal{X}_τ , which we track via entropy $H(q_k) = -\mathbb{E}_{x \sim q_k}[\log q_k(x)]$. Crucially, for both families this entropy is measured over the *solution space* \mathcal{X}_τ , not over any intermediate representation. For LLM agents, whose outputs are token sequences, q_k^{llm} denotes the marginal distribution over solutions obtained by integrating out the token sequences: $q_k^{\text{llm}}(x) = \sum_{s: \text{decode}(s)=x} p_\theta(s | c_k)$, where s is a token sequence and $\text{decode}(\cdot)$ maps it to a candidate $x \in \mathcal{X}_\tau$. This ensures that $H(q_k^{\text{llm}})$ and $H(q_k^{\text{bbo}})$ are both defined over the same space and are directly comparable.

Black-Box Optimization: In BBO, proposals depend on the evaluation history through an internal state ϕ_k :

$$\begin{aligned} q_k^{\text{bbo}}(x) &= q(x | \mathcal{D}_k, \phi_k), \\ \phi_{k+1} &= U(\mathcal{D}_{k+1}, \phi_k). \end{aligned} \quad (2)$$

Each new observation updates ϕ_k , shrinking predictive uncertainty $\sigma_k(x)$ in explored regions. The standard Upper Confidence Bound acquisition (Snoek et al., 2012): $\alpha_{\text{UCB}}(x) = \mu_k(x) + \kappa \sigma_k(x)$ converts this updated uncertainty into the next proposal: as σ_k concentrates, so does q_k^{bbo} , and $H(q_k^{\text{bbo}})$ decreases¹. The coefficient κ provides a task-adaptive handle on the exploration-exploitation trade-off independently of any prior.

However, BBO proposals are generated through a parametric family $\mathcal{Q} = \{q(\cdot | \phi) : \phi \in \Phi\}$, so the entropy reduction guarantee holds only *within the reachable set* of \mathcal{Q} , not over all of \mathcal{X}_τ .

LLM Agent: In an LLM agent, pretrained weights θ remain fixed during inference:

$$\begin{aligned} x_{k+1} &\sim q_k^{\text{llm}}(x | \mathcal{D}_k, c_k; \theta), \\ c_{k+1} &= \pi(c_k, \mathcal{D}_{k+1}, \mathcal{G}), \end{aligned} \quad (3)$$

where π is the agent policy and \mathcal{G} the task goal. That is, BBO adapts by updating optimizer state while an LLM agent adapts by updating context. Feedback can shift q_k^{llm} through context updates, but the frozen weights impose a c_k -independent lower bound on $H(q_k^{\text{llm}})$: there exists $H_\theta > 0$ such that for all c_k $H(q_k^{\text{llm}}) \geq H_\theta$, reflecting the support that θ places over \mathcal{X}_τ regardless of accumulated feedback. When the pretrained prior is dense over the target representation, H_θ is low and feedback steers proposals effectively, when the prior is sparse, entropy cannot fall below H_θ irrespective of how much feedback accumulates.

Practical implications: Both families exhibit structural constraints. LLM agents are bounded below in entropy by the coverage of the pretrained prior θ over \mathcal{X}_τ . BBO methods are bounded by the expressiveness of the chosen parametric family \mathcal{Q} over the same space. Although neither approach is superior, these constraints explain why hybrid methods are now emerging in practice, which combine LLM-guided proposal generation with structured search (Ferreira et al., 2026; Novikov et al., 2025) and how reinforcement learning is applied to lower H_θ via updating model weights (Surina et al., 2025).

¹Note that this entropy-reduction view may also apply to non-Bayesian optimizers such as CMA-ES (Hansen, 2016), whose proposal distribution (a multivariate normal) contracts as its internal state ϕ_k (mean, step-size, covariance) converges.

3 LLMs as BBO Optimizers

3.1 Methods and Evaluation for BBO Problems

We compare LLM-based search against three baselines: (1) **CMA-ES** (Hansen, 2016) implemented via Optuna (Akiba et al., 2019), (2) **Centaur** (Ferreira et al., 2026), a hybrid of CMA-ES and LLM system, and (3) **MCTS**, an LLM discovery enhanced with Monte Carlo Tree Search.

Problems. We evaluate on four task sets, three two-dimensional and one five-dimensional. The first set contains 100 2d synthetic problems with unknown closed-form **Functions** that have multiple local minima. The second set contains 100 2d problems based on equations from **Physical** dynamical systems. The third and fourth sets come from the **BBOB** benchmark (Finck et al., 2009), and represent 48 2d and 48 5d problems. All problems are bounded by $[-5, 5]$ through all axes.

Methods: For each problem, we evaluate all methods under the same 50-trial budget. For pure LLM and hybrid methods we use two LLMs `gpt-oss-120b` and `DeepSeek-V3.2 (685B)`. (1) *Pure LLM* is a sequential black-box proposer: at each step, it receives only the search history containing previous proposals, corresponding values and task prompt which includes search bounds, and returns the next candidate point. (2) *CMA-ES* (Hansen, 2016), chosen for its interpretable Gaussian state (mean, step-size, covariance), adapts from objective feedback. (3) *Centaur* (Ferreira et al., 2026) enables true co-adaptation by letting the LLM override CMA-ES proposals while CMA-ES learns from them, unlike other hybrids (Liu et al., 2024). (4) *LLM-MCTS* wraps the LLM proposer in a Monte Carlo Tree Search (Coulom, 2006) scaffold: each expansion selects a node via UCB1 (Kocsis and Szepesvári, 2006), prompts the LLM with the root-to-node path as context, samples k candidate points in parallel, attaches all k as children of the selected node, and back-propagates the minimum child loss through the ancestor chain.

Prompt templates for hybrid and pure LLMs experiments are provided in Appendix C.

Evaluation metrics. We summarize optimizer behavior over the 50-trial budget through three complementary quantities: *best step*, the trial at which the best loss is first attained (measuring convergence speed); *coverage*, the fraction of the search domain probed by the query sequence (measuring exploration breadth); and *normalized trajectory length*, the ratio of end-to-end displacement to total path length (measuring directional consistency, with $L = 1$ for a perfectly linear path and $L \approx 0.14$ for an isotropic random walk at $K = 50$). Full definitions are provided in Appendix D.

3.2 Results for LLMs as BBO Optimizer

Table 1 reports pairwise win counts, average best step, coverage Cov_{50} , and normalized trajectory length L . Figure 2 shows coverage over steps. Together, they reveal three distinct exploration regimes:

1. **LLMs act greedily, which suffices in 2D but breaks in higher dimensions.** LLMs win on *Functions*, where many local minima make greedy descent toward any plausible basin sufficient. On *Physical* tasks, however, where optima are isolated and exploration is necessary, both models fail. Low **Coverage** and high L indicate long, locally-confined trajectories rather than broad search critical for **BBOB-5D**, where both LLMs lose to CMA-ES and Centaur.
2. **MCTS represents the opposite extreme.** It covers the domain rapidly but exhausts its budget on exploration, rarely exploiting promising regions, though we note this is partly a consequence of our hyperparameter choices.
3. **CMA-ES and Centaur have the best balance.** They demonstrate moderate **Coverage** and trajectory length, achieving the strongest average performance across tasks.

When prompted to act as Bayesian optimizers, LLMs still behaved greedily (Figure 3). Inspection of the models’ chain-of-thought confirms that they attempt to mimic a gradient strategy to justify each successive proposal (Table 2). We further investigate whether earlier steps influence model decisions or whether the model anchors solely on the current best result. To this end, we sampled 10 points on a two-dimensional sphere and then asked each model to propose 5 additional steps. In every case, the next proposal was closest to the current best solution rather than to the most recent step. Results are shown in Figure 3. Experimental protocols and prompt templates are provided in Appendix E.

The central conclusion is that LLM search is inherently greedy, we speculate this may be a consequence of the training objective, in which the model is rewarded for predicting the single most likely next token. However, we acknowledge it is still possible that this behavior arises from exposure to numerical optimization routines in the training data, which may bias the model toward gradient-like strategies. In the next section we demonstrate similar behavior in a different domain.

4 Kernel Optimization

This section evaluates three claims about how the LLM prior shapes kernel generation.

1. Zero-shot LLM generation does not adapt to input size but collapses to a fixed prior regardless of prompt conditioning.

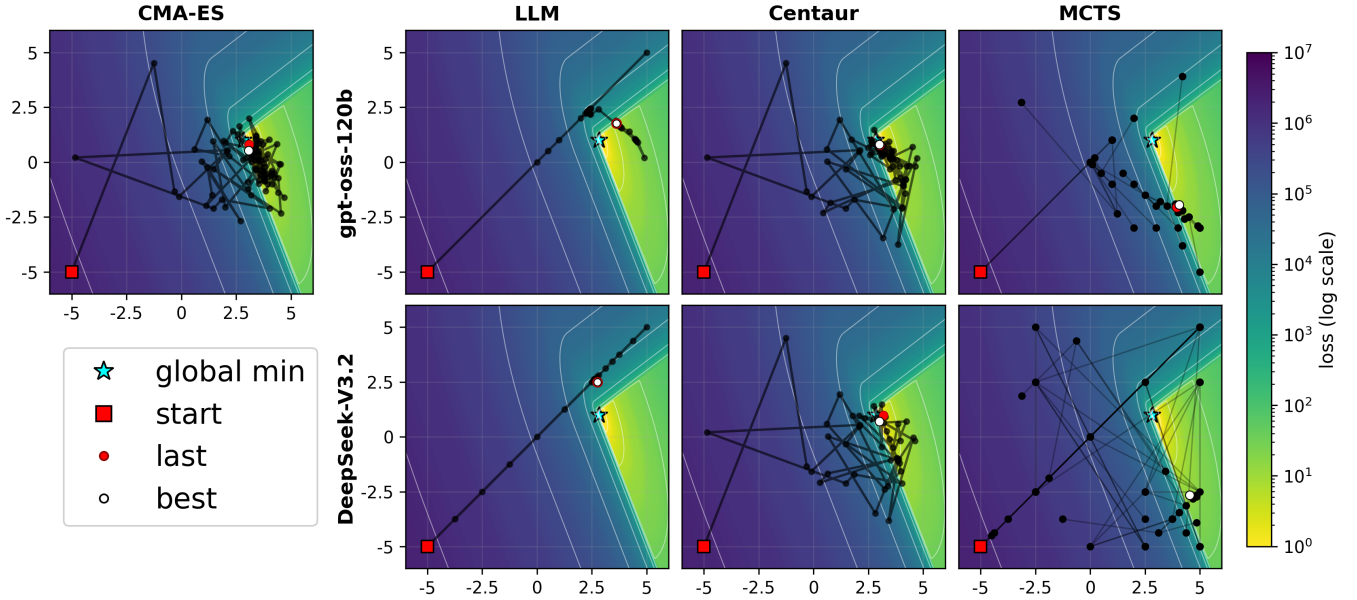


Figure 1: An example of optimization traces. An LLM often follows a greedy, line-like trajectory that either converges quickly or commits to a suboptimal direction. Additional illustrations of two dimensional BBO trajectories are presented in Appendix M.

Table 1: Results for BBO optimization. Entries in the *LLM vs optimizer* block are pairwise win counts in the form [*plain-LLM wins vs Method wins*], with the larger count shown in bold. Each following block presents different metric for each method. Methods: LLM, CMA-ES (CME), Centaur (Cent.), MCTS. Metrics: average best step, final coverage Cov_{50} (%), and normalized trajectory length L , all definitions are provided in Appendix D.

Model	Task	LLM vs optimizer			Avg. best step				Coverage (%)				L			
		CME	Cent.	MCTS	LLM	CME	Cent.	MCTS	LLM	CME	Cent.	MCTS	LLM	CME	Cent.	MCTS
gpt-oss	Functions	78 vs 22	75 vs 25	83 vs 17	42.8	31.8	37.7	27.6	10.9	44.8	45.3	93.4	0.72	0.16	0.16	0.16
	Physical	37 vs 63	29 vs 71	49 vs 51	46.7	35.3	44.1	33.4	22.4	71.2	71.4	93.9	0.67	0.17	0.19	0.17
	BBOB	23 vs 25	18 vs 30	25 vs 23	40.0	36.2	39.1	36.1	11.7	37.1	33.1	82.1	0.68	0.18	0.18	0.27
	BBOB-5D	11 vs 37	11 vs 37	19 vs 29	46.7	34.7	43.6	42.3	11.8	41.0	48.5	69.8	0.60	0.11	0.14	0.32
DeepSeek	Functions	80 vs 20	81 vs 19	88 vs 12	40.7	31.8	37.5	30.4	24.1	44.8	41.8	97.1	0.61	0.16	0.16	0.15
	Physical	42 vs 58	36 vs 64	65 vs 35	43.3	35.3	42.6	30.3	28.0	71.2	68.8	99.3	0.63	0.17	0.21	0.13
	BBOB	28 vs 20	25 vs 23	33 vs 15	35.8	36.2	38.0	31.6	33.4	37.1	35.7	97.2	0.57	0.18	0.17	0.19
	BBOB-5D	12 vs 36	9 vs 39	23 vs 25	36.2	34.9	41.3	24.7	17.3	41.1	51.8	97.9	0.42	0.11	0.12	0.14

Table 2: Verbatim reasoning excerpts recorded after step 10 for both models and both prompt regimes. In every condition the model describes a gradient strategy to justify a local perturbation of the best seen point.

Prompt regime	gpt-oss-120b	DeepSeek-V3.2
Black-box	“Use some heuristic: maybe gradient descent approximated. [...] propose slight variations [around the best point].”	“We can try to explore around minima. Use some local search: maybe gradient descent approximated. [...] try slight perturbations.”
BO-style prompt	“Could try gradient -like: maybe lower both slightly? [...] pick a promising point near best but not same.”	“Propose a point near best but slightly different to refine gradient : maybe (0.57,0.46) or (0.59,0.48).”

- Iterative feedback-loop optimization is representation-dependent: LLM priors over CUDA improve results under feedback, whereas sparser TVM IR prior degrades results.
- The prior-alignment advantage of LLM agents over the prior-free TVM MetaSchedule disappears when the input-size distribution shifts away from the

benchmark’s canonical regime.

Both experiments use `gpt-oss-120b` and `Qwen3-Coder-Next` (80B). Auxiliary calls are sampled at temperature 0.7 and code-generation calls at 0.1. For `gpt-oss-120b` we use medium reasoning effort. All kernel generation experiments were conducted on a server with 8 NVIDIA A100-SXM4-80GB GPUs, CUDA 12.6, PyTorch 2.9.0, and an AMD EPYC 7513 32-Core CPU (2.0 TiB RAM).

4.1 Shape Bias Analysis

Setup. We construct a shape grid for three kernels (`Softmax`, `Matmul_with_transposed_A`, and a fused convolutional kernel) spanning 10 sizes from small to large. Each prompt includes the Python reference implementation with concrete input sizes. We evaluate two instruction regimes: *implicit* (size stated once in the task description) and *explicit* (same, plus a direct instruction to attend to the listed sizes). We sample 20 zero-shot kernels per grid point at $T \in \{0.1, 0.5, 0.8\}$, recording pass-rate and the dominant tiling parameters

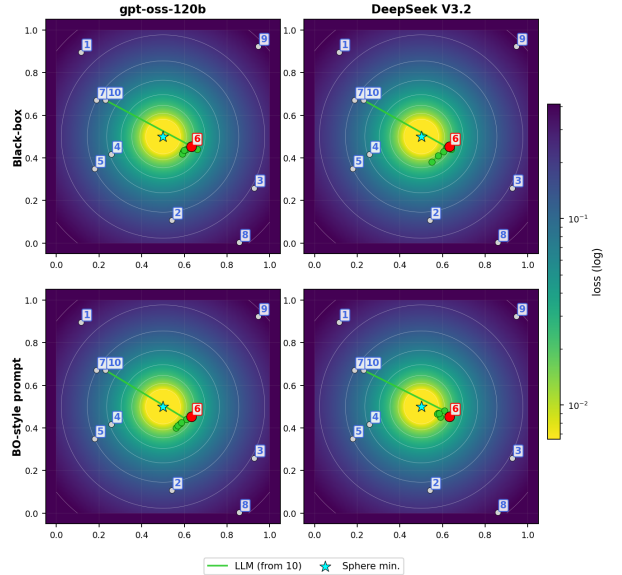
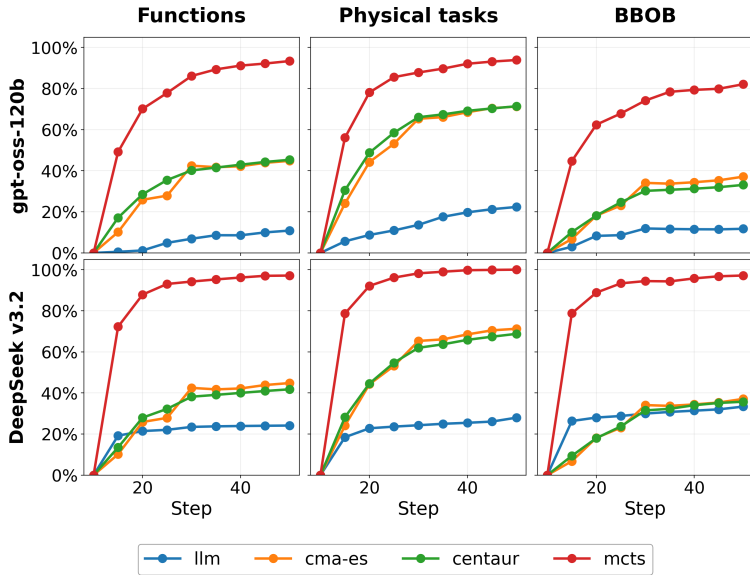


Figure 2: Per-step coverage Cov_k (Eq. 10) of the search domain under the four optimization settings, evaluated every five steps of the 50-trial budget. Columns correspond to task families (Functions, Physical tasks, BBOB); rows correspond to the two LLM backbones (gpt-oss-120b, top; DeepSeek-V3.2, bottom). The pure-LLM proposer saturates well below all other methods, CMA-ES and Centaur share a common mid-range regime, and LLM-MCTS attains the highest coverage in every family.

Figure 3: Columns show the two backbones, rows show the standard prompt and *BO-pretending* prompt for LLMs. Steps 1-10 are uniform-random samples (white labeled circles), the best of these is highlighted in red. The green segment marks future LLM-proposed steps 11-15 and the cyan star is the true minimum. LLMs next proposal is always close to the best in history point.

emitted. Full prompt templates are in Appendix F.

Results. The left panels of Figure 4 show pass-rate curves that are essentially flat across the entire size grid for both models and at all three temperatures. The explicit and implicit prompt conditions produced nearly identical curves, and Figure 4 therefore shows their average.

The right panels show the main pattern. The parameters that control hardware performance (block size, tile size, vector width, and unroll factor) are fixed across the whole grid, while details such as variable names and loop ordering can differ. These parameters collapse to the same few modes regardless of size or temperature (detailed results are presented in Appendix G).

The flat pass-rate therefore indicates that the model produces the same hardware-level configuration for every input, which compiles and runs correctly but is not adapted to the shape.

4.2 Iterative Hardware-Aware Kernel Optimization with Feedback

Experimental Setup. In this section, we evaluate how LLMs optimize kernels in terms of correctness and speed under two code representations, two optimization pipelines, and two size regimes.

Code Representations.

We employ two code representations CUDA and TVM IR that differ substantially in LLM pretraining corpus size (Figure 5).² For CUDA, the model

translates a PyTorch reference to a CUDA kernel. For TVM IR, the reference is an *unscheduled* TVM-TIR program derived from the same PyTorch model via automated conversion (ONNX→Relax→TIR, with schedule annotations stripped), so the computation is already correctly implemented. This allows us to have two computationally equivalent tasks but represented differently. The pipeline is described in Appendix H.

Size Regimes.

We evaluate two input-size regimes using problems from KernelBench: the *base* regime uses the original shapes and *small-input* regime uses the substantially reduced sizes (e.g. matrix multiplication shrinks from $M=2048, K=8192, N=4096$ to $M=128, K=512, N=256$). More examples are provided in Appendix I). All experiments cover KernelBench levels one and two, evaluated on 100 kernels per level in each size regime.

Baselines.

`torch.compile` is the main performance reference, all speedups are reported relative to it. TVM MetaSchedule is the primary non-LLM baseline; it updates its search state solely from observations with no pretrained prior, making it a direct representative of the BBO family (Section 2).

Agent Pipelines.

Two pipelines are compared. The **Sampling Agent** generates five candidates independently, converts each outcome into structured feedback, and conditions a representative of the pretraining corpora of the models evaluated here.

²Token counts are from The Stack (2022), which is repre-

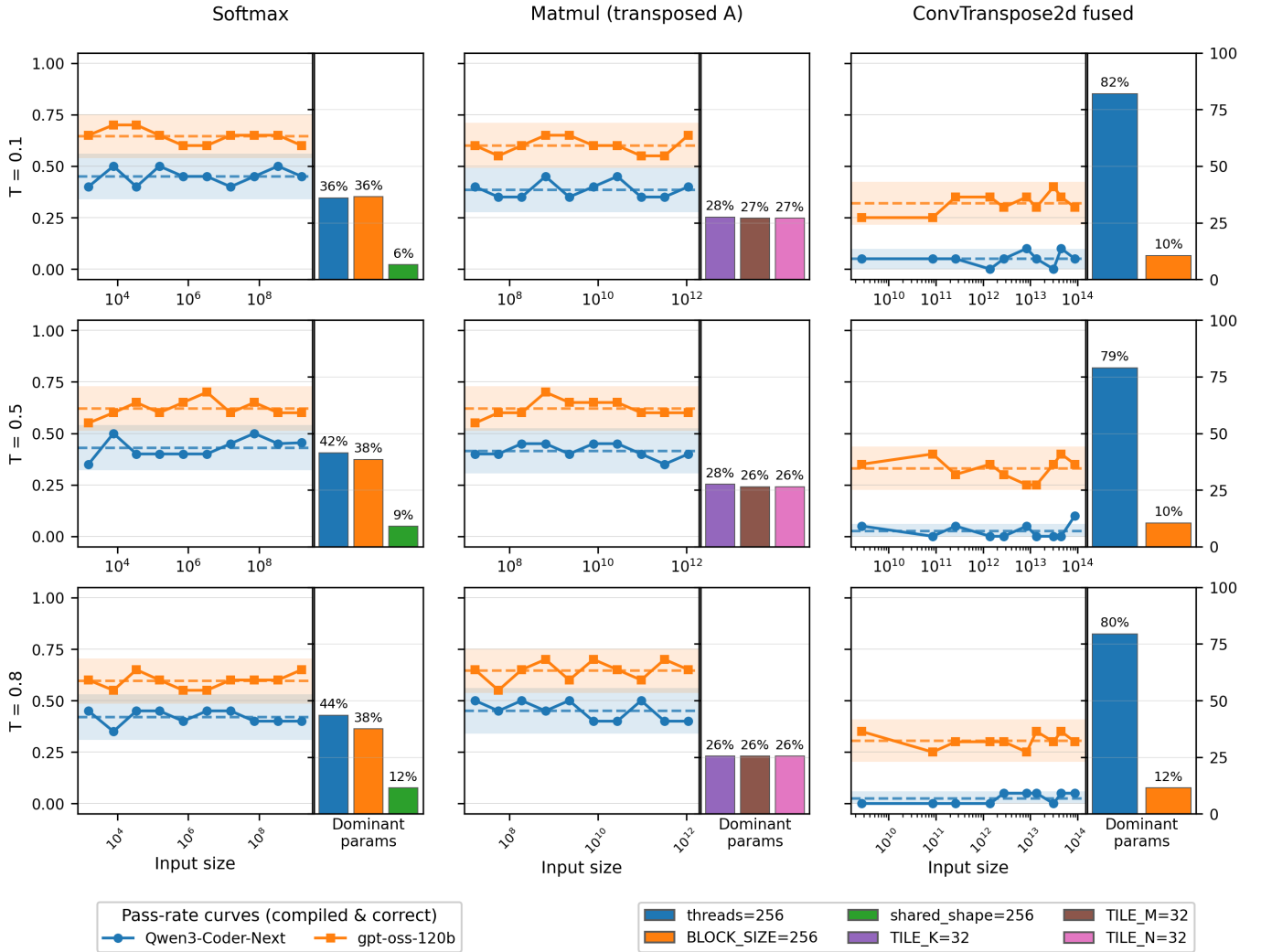


Figure 4: Zero-shot pass-rate and dominant kernel parameters across shape grids for three kernels (**Softmax**, **Matmul** with transposed A , and a fused **ConvTranspose2d** kernel), evaluated at three temperatures ($T \in \{0.1, 0.5, 0.8\}$). *Left panel in each cell*: pass-rate vs. input size for two models (**Qwen3-Coder-Next**, blue; **gpt-oss-120b**, orange), averaged over explicit and implicit prompt conditions (both conditions yield indistinguishable curves, so only the average is shown). *Right panel in each cell*: frequency of the most common kernel parameter. Dominant parameters are stable across all temperatures.

sixth candidate on all five reference-candidate pairs. The **Feedback Loop** pairs an *advisor/diagnoser* agent with a *coder* over up to five sequential iterations, the advisor recommends further optimizations when the kernel is correct, or the diagnoser prescribes a fix when it is not. Detailed description is presented in Appendix J.

Results.

1. **Language prior determines whether feedback helps or hurts.** Figure 7 shows that CUDA remains stable under feedback. For **gpt-oss-120b**, the compiled-and-correct rate steadily improves across iterations. TVM IR behaves in the opposite way, as both the compiled-and-correct and correct-and-faster rates decrease when feedback accumulates. We attribute this to a language-prior bottleneck. Iterative feedback effectively steers proposals when the model has a dense prior over the target representation, but it destabilizes generation when that prior is sparse. Importantly, TVM IR starts

from a semantically stronger reference, namely a valid unscheduled program, yet its pass rate still declines. This confirms that the effect is driven by prior density rather than reference quality.

2. **Size prior determines who wins under distribution shift.** Figure 6 shows that on benchmark-native sizes the TVM IR Feedback Loop is roughly competitive with MetaSchedule. Under the small-input shift the pattern reverses: MetaSchedule wins on 69% and 67% of kernels for **gpt-oss-120b** and **Qwen3-Coder-Next** respectively, with the effect strongest on Level 2. The LLM feedback policy carries size-specific parameter biases calibrated to benchmark-native shapes; when the workload scale changes, those biases become misleading. MetaSchedule carries no such prior and searches freely in the shifted regime.
3. **Sequential feedback dominates parallel sampling.** Figure 8 shows iterative gain relative to

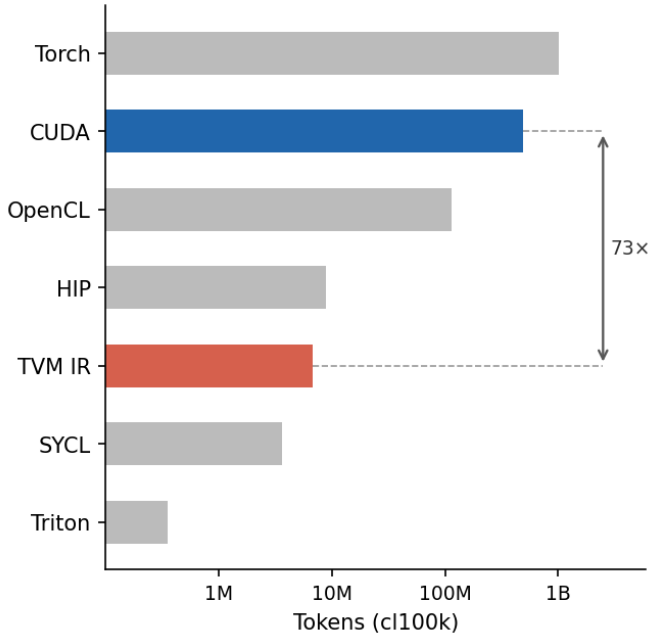


Figure 5: Token counts (cl100k tokenizer) for GPU-related code categories in The Stack (Kocetkov et al., 2023). The TVM corpus consists of Python files using TVM APIs. The x-axis is logarithmic.

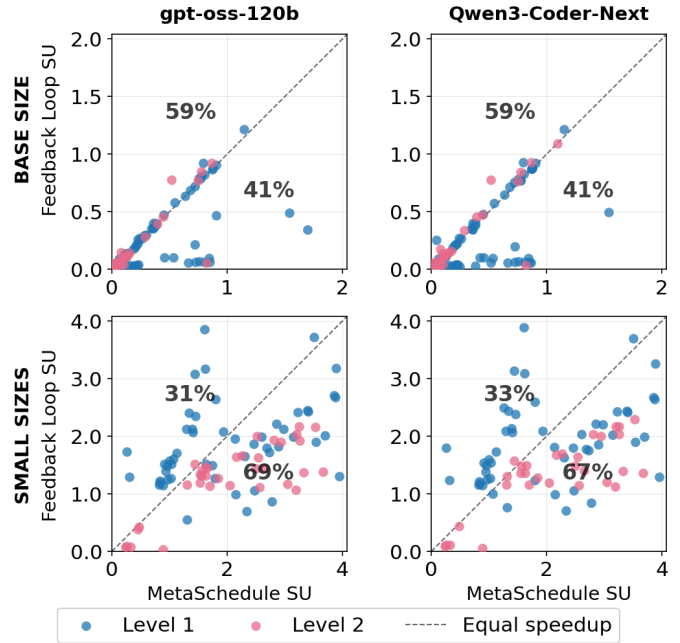


Figure 6: Per-kernel speedup: TVM MetaSchedule vs. TVM IR Feedback Loop. Points above the diagonal indicate kernels where Feedback Loop is faster; percentages show the fraction of kernels on each side of the diagonal.

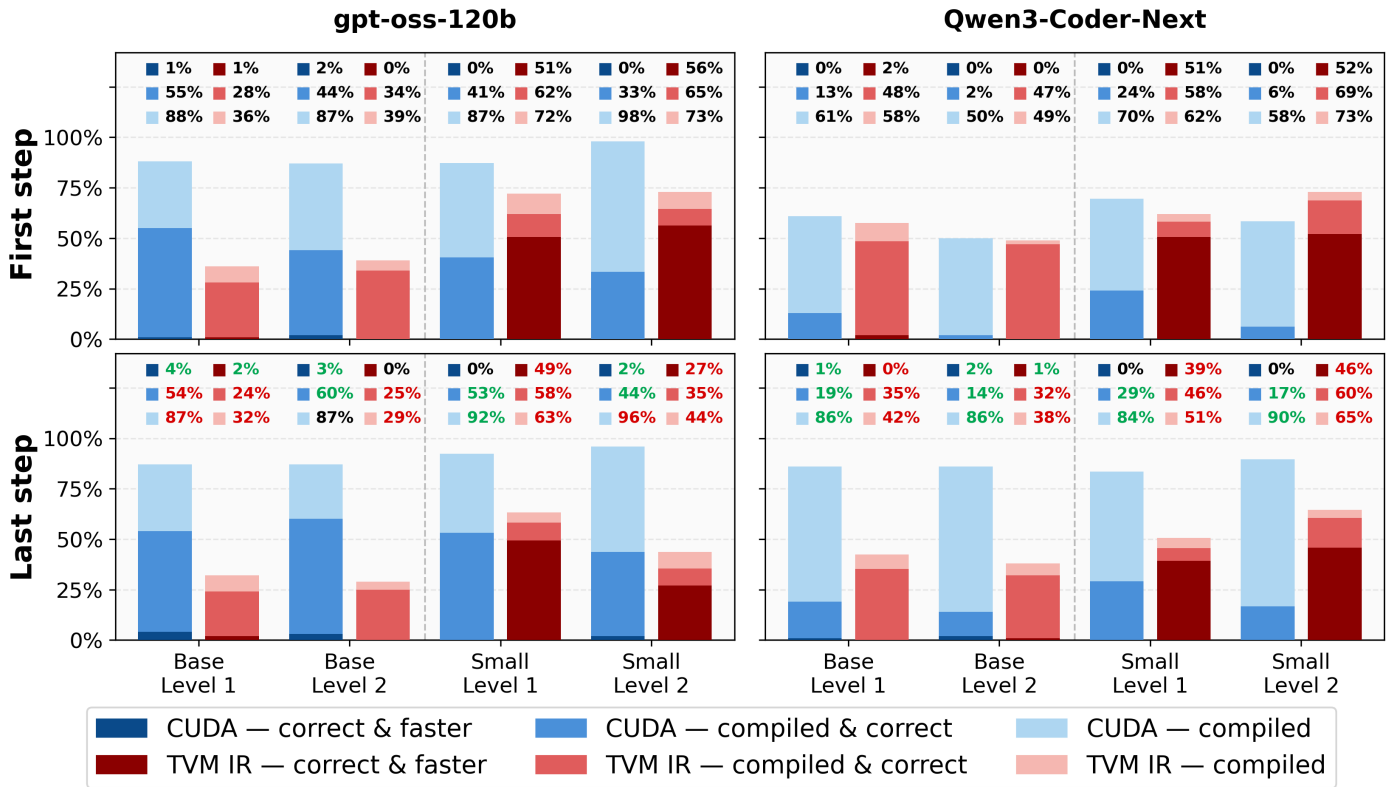


Figure 7: Feedback Loop validity and acceleration outcomes for CUDA and TVM IR generation. Bars show nested outcomes: compiled, compiled and correct, and correct and faster than torch.compile. Top row: iteration 1; bottom row: iteration 5. Blue: CUDA; red: TVM IR. Appendix K shows all five iterations.

the iteration-1 baseline. The Feedback Loop consistently outperforms the Sampling Agent under a matched LLM budget. The two converge only in the densest-prior corner (native-size CUDA), where aggregated context is rich enough to condition on effectively; elsewhere, the gap is substantial. Two

factors likely explain the Sampling Agent’s under-performance: an overloaded context window, and the fact that many small corrections from external, prior-independent signals outperform a single large update from cluttered context. Relative improvement over iteration 1 is larger for TVM IR, but

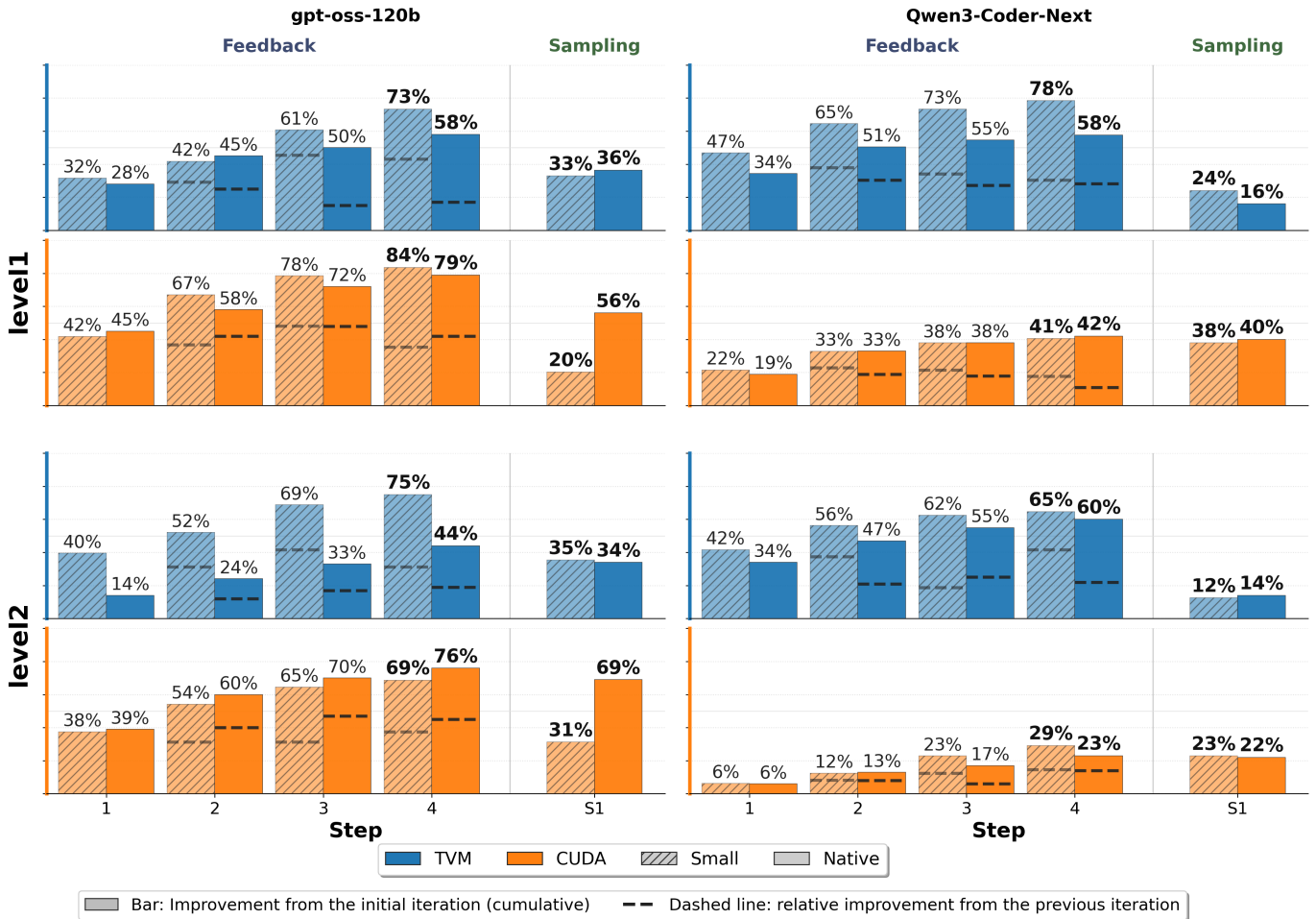


Figure 8: Iterative improvement relative to the first iteration under two agent architectures (Feedback Loop vs. Sampling Agent), two representations (TVM IR, CUDA), two models, and two size regimes (native, small). Feedback bars at iterations 2-5 show the cumulative fraction of kernels improved over iteration 1; dashed segments show per-step improvement. The Sampling column (S1) shows the single post-aggregation candidate.

only because CUDA starts from a stronger LLM-generated baseline and therefore has less headroom. This does not contradict the absolute degradation in Figure 7, because the kernels that improve and the kernels that degrade are not the same subsets.

Across the experiments, the same pattern holds:

- Zero-shot generation ignores stated input sizes because a strong code-generation prior overrides the prompt.
- Iterative feedback helps in CUDA and hurts in TVM IR, which is less represented in training data.
- TVM MetaSchedule overtakes the LLM agent under size shift.
- Agentic structure and feedback signals can amplify performance, but only where the pretrained prior is already aligned with the target solution space; they cannot compensate for its absence.

5 Discussion

In this section, we interpret our findings and discuss what they imply for discovery and optimization pipelines.

Prior alignment shapes context use. The greedy local search in BBO (Section 3.2) and the prior collapse in shape-conditioned kernel generation (Section 4) both

arise from the model conditioning on the part of the prompt most aligned with its prior. In BBO, the next decision is anchored to the best current value. In kernel generation, abundant high-likelihood examples cause the model to reuse common parameter modes instead of mapping the requested shape to specialized tile, vector-width, or unrolling choices. This is consistent with the entropy lower bound (Section 2): the model can refine only within its prior.

Feedback helps only when it fills the right gap.

In BBO, each evaluation directly reveals the unknown objective value at a queried point. In TVM IR, however, the key missing knowledge is how to construct a valid and efficient schedule. Compiler errors and profiling indicate whether a candidate failed or how fast it is, but they do not provide the scheduling patterns needed for improvement. This may explain why simply increasing the number of feedback iterations is often insufficient.

LLM exploration can be improved in three ways: (1) by adapting the prior via domain-specific RL (Dai et al., 2026), (2) by retrieving examples that contain informative patterns at inference time, and (3) by forcing exploration externally through agentic scaffolding.

Limitations and Broader Impact. Our study is limited to a few model families and standard benchmarks. Better kernel generation could reduce energy costs, but automatically generated code demands rigorous validation before production use.

6 Conclusion

This work argues that the central variable in agentic optimization is not whether feedback exists, but whether feedback can be absorbed by the model’s prior. Across BBO, shape-conditioning, and hardware optimization, we observe a common pattern: LLMs are strong prior exploiters and weak open-ended searchers. From this view, three takeaways follow.

First, feedback is representation-conditional: it is beneficial in dense-prior domains and can destabilize in sparse-prior ones. Second, sequential conditioning on concrete external signals is more effective than one-shot aggregation of many sampled trajectories at similar budget. Third, robust optimization pipelines should route adaptively: use LLM refinement where prior coverage is dense, and rely on task-adaptive search when distribution shift or sparse prior makes language-only adaptation unreliable.

References

Takuya Akiba, Shotaro Sano, Toshihiko Yanase, Takeru Ohta, and Masanori Koyama. 2019. [Optuna: A next-generation hyperparameter optimization framework](#). In *Proceedings of the 25th ACM SIGKDD International Conference on Knowledge Discovery & Data Mining*, pages 2623–2631. ACM.

Rémi Coulom. 2006. [Efficient selectivity and backup operators in Monte-Carlo tree search](#). In *Computers and Games (CG)*, pages 72–83. Springer.

Weinan Dai, Hanlin Wu, Qiyang Yu, Huan-Ang Gao, Jiahao Li, Chengquan Jiang, Weiqiang Lou, Yufan Song, Hongli Yu, Jiaye Chen, Wei-Ying Ma, Ya-Qin Zhang, Jingjing Liu, Mingxuan Wang, Xin Liu, and Hao Zhou. 2026. [CUDA agent: Large-scale agentic RL for high-performance CUDA kernel generation](#).

Fabio Ferreira, Lucca Wobbe, Arjun Krishnakumar, Frank Hutter, and Arber Zela. 2026. [Can llms beat classical hyperparameter optimization algorithms? A study on autoresearch](#).

Steffen Finck, Nikolaus Hansen, Raymond Ros, and Anne Auger. 2009. [Real-parameter black-box optimization benchmarking 2009: Noiseless functions definitions](#). Technical Report RR-6829, INRIA.

Xiangming Gu, Soham De, Michalis Titsias, Larisa Markeeva, Petar Veličković, and Razvan Pascanu. 2026. [The illusion of stochasticity in LLMs](#).

Nikolaus Hansen. 2016. [The CMA evolution strategy: A tutorial](#).

Sen Huang, Kaixiang Yang, Sheng Qi, and Rui Wang. 2024. [When large language model meets optimization](#). *Swarm and Evolutionary Computation*, 90:101663.

Valentin Khrulkov, Andrey V. Galichin, Denis Bashkirov, Dmitry Vinichenko, Oleg Travkin, Roman Alferov, Andrey Kuznetsov, and Ivan V. Oseledets. 2025. [Gigaevo: An open source optimization framework powered by llms and evolution algorithms](#).

Denis Kocetkov, Raymond Li, Loubna Ben Allal, Jia Li, Chenghao Mou, Yacine Jernite, Margaret Mitchell, Carlos Muñoz Ferrandis, Sean Hughes, Thomas Wolf, Dzmitry Bahdanau, Leandro von Werra, and Harm de Vries. 2023. [The stack: 3 TB of permissively licensed source code](#). *Transactions on Machine Learning Research (TMLR)*.

Levente Kocsis and Csaba Szepesvári. 2006. [Bandit based Monte-Carlo planning](#). In *European Conference on Machine Learning (ECML)*, pages 282–293. Springer.

Robert T. Lange, Yingtao Tian, and Yujin Tang. 2024. [Evolution transformer: In-context evolutionary optimization](#). In *Genetic and Evolutionary Computation Conference (GECCO)*, pages 575–578. ACM.

Robert Tjarko Lange, Qi Sun, Aaditya Prasad, Maxence Faldor, Yujin Tang, and David Ha. 2025. [Towards robust agentic CUDA kernel benchmarking, verification, and optimization](#).

Gang Liao, Hongsen Qin, Ying Wang, Alicia Golden, Michael Kuchnik, Yavuz Yetim, Jia Jiunn Ang, Chunli Fu, Yihan He, Samuel Hsia, Zewei Jiang, Dianshi Li, Uladzimir Pashkevich, Varna Puvvada, Feng Shi, Matt Steiner, Ruichao Xiao, Nathan Yan, Xiayu Yu, and 19 others. 2025. [KernelEvolve: Scaling agentic kernel coding for heterogeneous AI accelerators at Meta](#).

Tennison Liu, Nicolás Astorga, Nabeel Seedat, and Mihaela van der Schaar. 2024. [Large language models to enhance bayesian optimization](#). In *The Twelfth International Conference on Learning Representations*.

Alexander Novikov, Ngán Vu, Marvin Eisenberger, Emilien Dupont, Po-Sen Huang, Adam Zsolt Wagner, Sergey Shirobokov, Borislav Kozlovskii, Francisco J. R. Ruiz, Abbas Mehrabian, M. Pawan Kumar, Abigail See, Swarat Chaudhuri, George Holland, Alex Davies, Sebastian Nowozin, Pushmeet Kohli, and Matej Balog. 2025. [Alphaevolve: A coding agent for scientific and algorithmic discovery](#).

Anne Ouyang, Simon Guo, Simran Arora, Alex L. Zhang, William Hu, Christopher Ré, and Azalia Mirhoseini. 2025. [KernelBench: Can LLMs write efficient GPU kernels?](#) In *International Conference on Machine Learning (ICML)*.

Bernardino Romera-Paredes, Mohammadamin Barekatain, Alexander Novikov, Matej Balog, M. Pawan Kumar, Emilien Dupont, Francisco J. R. Ruiz, Jordan S. Ellenberg, Pengming Wang, Omar Fawzi, Pushmeet Kohli, and Alhussein Fawzi. 2024. [Mathematical discoveries from program search with large language models](#). *Nature*, 625:468–475.

Bobak Shahriari, Kevin Swersky, Ziyu Wang, Ryan P Adams, and Nando De Freitas. 2015. [Taking the human out of the loop: A review of bayesian optimization](#). *Proceedings of the IEEE*, 104(1):148–175.

Parshin Shojaee, Kazem Meidani, Shashank Gupta, Amir Barati Farimani, and Chandan K. Reddy. 2025. [LLM-SR: Scientific equation discovery via programming with large language models](#). In *International Conference on Learning Representations (ICLR)*.

- Jasper Snoek, Hugo Larochelle, and Ryan P. Adams. 2012. Practical bayesian optimization of machine learning algorithms. In *Advances in Neural Information Processing Systems (NeurIPS)*, pages 2960–2968.
- Kaya Stechly, Karthik Valmeekam, and Subbarao Kambhampati. 2024. Chain of thoughtlessness? An analysis of CoT in planning. In *Advances in Neural Information Processing Systems (NeurIPS)*.
- Yiyou Sun, Shawn Hu, Georgia Zhou, Ken Zheng, Hananeh Hajishirzi, Nouha Dziri, and Dawn Song. 2025. OMEGA: can llms reason outside the box in math? evaluating exploratory, compositional, and transformative generalization.
- Anja Surina, Amin Mansouri, Lars Quaedvlieg, Amal Seddas, Maryna Viazovska, Emmanuel Abbe, and Caglar Gulcehre. 2025. Algorithm discovery with llms: Evolutionary search meets reinforcement learning.
- Ziyang Xiao, Jingrong Xie, Lilin Xu, Shisi Guan, Jingyan Zhu, Xiongwei Han, Xiaojin Fu, WingYin Yu, Han Wu, Wei Shi, Qingcan Kang, Jiahui Duan, Tao Zhong, Mingxuan Yuan, Jia Zeng, Yuan Wang, Gang Chen, and Dongxiang Zhang. 2025. [A survey of optimization modeling meets LLMs: Progress and future directions](#). In *International Joint Conference on Artificial Intelligence (IJCAI)*, pages 10742–10750. ijcai.org.
- Chengrun Yang, Xuezhi Wang, Yifeng Lu, Hanxiao Liu, Quoc V. Le, Denny Zhou, and Xinyun Chen. 2024. Large language models as optimizers. In *International Conference on Learning Representations (ICLR)*.
- Zonglin Yang, Wanhao Liu, Ben Gao, Tong Xie, Yuqiang Li, Wanli Ouyang, Soujanya Poria, Erik Cambria, and Dongzhan Zhou. 2025. MOOSE-Chem: Large language models for rediscovering unseen chemistry scientific hypotheses. In *International Conference on Learning Representations (ICLR)*.
- Xinhao Zhang, Xi Chen, François Portet, and Maxime Peyrard. 2026. What makes an LLM a good optimizer? A trajectory analysis of LLM-guided evolutionary search.
- Chengshuai Zhao, Zhen Tan, Pingchuan Ma, Dawei Li, Bohan Jiang, Yancheng Wang, Yingzhen Yang, and Huan Liu. 2025. Is chain-of-thought reasoning of llms a mirage? A data distribution lens.
- Zihan Zheng, Zerui Cheng, Zeyu Shen, Shang Zhou, Kaiyuan Liu, Hansen He, Dongruixuan Li, Stanley Wei, Hangyi Hao, Jianzhu Yao, Peiyao Sheng, Zixuan Wang, Wenhao Chai, Aleksandra Korolova, Peter Henderson, Sanjeev Arora, Pramod Viswanath, Jingbo Shang, and Saining Xie. 2025. Livecodebench pro: How do olympiad medalists judge llms in competitive programming?

Appendix

The appendix is organized as follows. Appendix A surveys related work on LLM reasoning, LLM-based optimization, and LLM-based kernel generation. Appendix B formalizes the entropy reduction guarantee for BBO and the entropy floor for LLM agents. Appendix C lists the exact prompt templates used in the synthetic BBO comparison. Appendix D defines the evaluation metrics for the pure BBO experiments. Appendix E details the experimental protocol for the greedy-gradient probe. Appendix F provides the prompt templates for shape-conditioned zero-shot generation. Appendix G tabulates the dominant zero-shot parameter modes across temperatures. Appendix H describes the pipeline for constructing the unscheduled TVM-TIR reference module. Appendix I lists the tensor shapes used across all benchmark regimes. Appendix J illustrates the two agentic pipeline architectures via flowcharts and a summary table. Appendix K expands the feedback-loop validity figure to all five iterations. Appendix L reports additional TVM MetaSchedule vs. `torch.compile` size sweeps. Appendix M provides per-task BBOB optimization trace plots.

A Related Work

We survey prior work across three threads directly relevant to our study: (i) the limits of LLM reasoning under distributional shift, (ii) LLMs as optimization operators and search primitives, and (iii) LLM-based approaches to GPU kernel generation.

LLM Reasoning. A growing body of work challenges the assumption that frontier LLMs possess robust, generalizable reasoning, converging instead on a picture of brittle pattern matching that degrades rapidly under distributional shift. (Stechly et al., 2024) provide an early and influential demonstration of this through careful experimentation in the Blocksworld planning domain. Varying both the generality of in-context examples and the complexity of test problems, they find that Chain of Thought (CoT) prompting yields meaningful gains only when prompts are narrowly tailored to the specific problem class and that even these gains collapse quickly as problem size grows beyond what was demonstrated. (Zhao et al., 2025) extend and formalize this critique through an explicit distributional lens. Introducing a controlled training environment, they demonstrate that CoT behavior reflects a structured bias learned from in-distribution data, whose effectiveness is fundamentally bounded by the degree of mismatch between training and test distributions. (Sun et al., 2025) evaluates out-of-distribution generalization along three axes exploratory, compositional, and transformative using programmatically generated problem templates with adjustable complexity. Evaluations of frontier models reveal sharp, monotonic accuracy degradation as complexity increases. Crucially, reinforcement learning fine-tuning on low-complexity data yields strong in-distribution gains but provides only limited and rapidly plateauing improvements out-of-distribution, with transformative generalization showing virtually no improvement at all. In the domain of competitive programming, (Zheng et al., 2025) corroborate these findings using a contamination-free benchmark of 584 problems drawn from Codeforces, ICPC, and IOI, continuously updated and annotated by Olympiad medalists. Even the best reasoning models achieve only 53% accuracy on medium-difficulty problems and 0% on hard problems, with failures concentrated on observation-heavy problems that require novel insights rather than the recall of known techniques. Fine-grained error analysis further reveals that conceptual failures dominate over implementation bugs, and that tool augmentation accounts for a substantial share of performance gains that do not reflect native reasoning ability. (Gu et al., 2026) question whether LLMs can stochastically explore environments by evaluating their ability to perform independent and sequential sampling of random numbers, finding that both approaches fail standard independence tests. However, the authors show that models can reliably *convert* externally provided random seeds to target distributions suggesting that the failure lies not in distributional understanding but in autonomous random generation. This knowing-doing gap offers a partial explanation for why tool augmentation so consistently boosts LLM performance in agentic settings.

LLM-Based Optimization. A complementary line of research reframes LLMs from problem-solvers to search operators, algorithm designers, and formal modelers within optimization loops (Huang et al., 2024). (Yang et al., 2024) pioneered the use of LLMs as iterative optimizers via Optimization by PROMpting (OPRO), while subsequent work has expanded this to using LLMs for translating natural language directly into rigorous mathematical optimization models (Xiao et al., 2025). When deployed as evolutionary search operators, trajectory analyses reveal that effective LLM optimizers diverge significantly from general reasoning behaviors; (Zhang et al., 2026) find that strong optimizers act as *local refiners*, producing frequent incremental improvements while maintaining a localized search region, whereas high novelty often leads to semantic drift without fitness gains. This behavioral nuance is reflected in empirical benchmarks: (Ferreira et al., 2026) show that classical algorithms like CMA-ES consistently outperform pure LLM agents in fixed hyperparameter spaces, though hybrid approaches that share the classical optimizer’s internal state (e.g., their proposed **Centaur** framework) achieve state-of-the-art results by letting the LLM apply domain knowledge to well-guided proposals. Architecturally,

this fusion is formalized by (Lange et al., 2024), who introduce the Evolution Transformer to distill evolutionary strategy updates into a causal attention mechanism, offering a structured alternative to purely text-based LLM search.

LLM-Based Kernel Generation. A recurring pattern is the pairing of LLMs with explicit exploration mechanisms. A notable production-oriented system is **KernelEvolve** (Liao et al., 2025), developed for generating optimized kernels across heterogeneous accelerators (NVIDIA, AMD, MTIA). It integrates tree search, agentic retrieval, knowledge base of hardware constraints, and a profiling feedback. However, the source code is proprietary, and the paper includes no ablation studies. Consequently, it remains unclear which components critically contribute to the reported gains. An open-source counterpart is KernelEvo, built on the GigaEvo evolutionary algorithm framework (Khruikov et al., 2025). It provides an implementation of LLM-guided evolutionary kernel generation. Yet it lacks a peer-reviewed paper, systematic evaluation and any ablation studies. **CUDA Agent** (Dai et al., 2026) develops a large-scale reinforcement learning system for CUDA kernel generation, using a synthetic dataset of fused operators, a structured agent toolset, and PPO with multi-stage warm-up. The system reports strong results on KernelBench. However, the work is limited to CUDA and lacks comparison with classical black-box optimizers (e.g., TVM MetaSchedule). Broadly, three strategies dominate: (i) tree search, (ii) population-based evolutionary diversification, and (iii) reinforcement learning that adapts the model weights themselves rather than only the context.

B Entropy Reduction: BBO Guarantee and LLM Entropy Floor

This section formalizes the key asymmetry between the two paradigms studied in the paper. We prove that Bayesian BBO admits a per-step entropy reduction guarantee in expectation-its proposal distribution narrows monotonically as observations accumulate-while an LLM agent is subject to an irreducible entropy floor imposed by its frozen weights and pretraining distribution. The floor is small for well-represented languages such as CUDA and large for sparse ones such as TVM IR, directly explaining the performance gap observed empirically.

We state formally why Bayesian BBO admits a per-step entropy reduction guarantee in expectation, and why an LLM agent is instead subject to an irreducible entropy floor.

Setup. Both methods share the outer loop of Section 2. At step k , each method maintains a proposal distribution q_k over \mathcal{X}_τ , draws a candidate $x_{k+1} \sim q_k$, observes $y_{k+1} = F_\tau(x_{k+1})$, and constructs q_{k+1} . A good optimizer is one for which

$$\mathbb{E}[H(q_{k+1}) \mid \mathcal{D}_k] \leq H(q_k), \quad (4)$$

where the expectation is over the randomness of the next observation (x_{k+1}, y_{k+1}) .

BBO satisfies (4). Let $q_k = p(x^* \mid \mathcal{D}_k)$ be the Bayesian posterior over the optimal point after k observations. By the definition of conditional entropy (tower property),

$$\begin{aligned} \mathbb{E}[H(q_{k+1}) \mid \mathcal{D}_k] &= \mathbb{E}_{x_{k+1}, y_{k+1}}[H(p(x^* \mid \mathcal{D}_k, x_{k+1}, y_{k+1}))] \\ &= H(x^* \mid \mathcal{D}_k, x_{k+1}, y_{k+1}) \\ &\leq H(x^* \mid \mathcal{D}_k) = H(q_k). \end{aligned} \quad (5)$$

The inequality uses $H(X \mid Y, Z) \leq H(X \mid Y)$: conditioning on additional observations cannot increase entropy. No assumption about F_τ or the structure of \mathcal{X}_τ is required.

LLM agents do not satisfy (4) in general. In an LLM agent the proposal distribution is not a posterior but a conditional of the frozen model:

$$q_k(x) = p_\theta(x \mid c_k, \mathcal{G}), \quad \theta \text{ fixed.} \quad (6)$$

After a context update $c_{k+1} = \pi(c_k, \mathcal{D}_{k+1}, \mathcal{G})$, the new distribution is $q_{k+1}(x) = p_\theta(x \mid c_{k+1}, \mathcal{G})$. The proof above does not apply for two reasons.

(i) *No Bayesian update.* The mapping $c_k \mapsto q_k$ is mediated by the frozen weights θ ; it is not a conditioning operation on a shared probability space. The inequality $H(X \mid Y, Z) \leq H(X \mid Y)$ applies only to proper conditional distributions.

(ii) *Frozen weights impose a strictly positive entropy floor.* Because θ is fixed, the set of distributions reachable by any context is

$$\mathcal{Q}_\theta = \{p_\theta(\cdot \mid c, \mathcal{G}) : c \in \mathcal{C}\}, \quad (7)$$

where \mathcal{C} denotes all contexts fitting within the model’s finite context window of length L_{\max} . Since the vocabulary and window length are both finite, \mathcal{C} is a finite set, and \mathcal{Q}_θ is a finite collection of distributions on the probability simplex. The entropy H is continuous on the simplex, so it attains its minimum over \mathcal{Q}_θ :

$$H_\infty(\theta, \mathcal{X}_\tau) = \min_{q \in \mathcal{Q}_\theta} H(q) \geq 0. \quad (8)$$

The strict inequality $H_\infty > 0$ holds whenever no context c drives $p_\theta(\cdot | c, \mathcal{G})$ to a point mass on any single $x \in \mathcal{X}_\tau$. This is the case precisely when \mathcal{X}_τ is sparsely covered by θ 's pretraining corpus: the model has not seen enough valid programs in \mathcal{X}_τ to assign probability 1 to any one of them, regardless of the prompt. For CUDA kernels, which are well-represented in pretraining, H_∞ is small and context updates can drive $H(q_k)$ close to zero efficiently. For TVM IR schedules, which are rare in pretraining, H_∞ is large and the model cannot concentrate its output below that floor no matter how much feedback is added to the context.

C Prompt Templates for the Synthetic BBO Comparison

This section reports the exact prompt templates used when asking the LLM to act as a black-box optimizer in the synthetic comparison from Section 3.2.

Two-dimensional function optimization.

You are optimizing an unknown black-box function.
 Goal: suggest x and y that minimize this function (smaller is better).
 Search bounds: x and y must be in [0, 1].
 Trial number: <trial_num>.
 Current best loss: <best_loss>.
 History of all previous attempts (step | x | y | loss):
 <history_lines>
 Important: do NOT repeat any previous (x, y) pair from history.
 Always propose a new point that was not tried before.
 Return ONLY JSON in this exact format: {"x": <float>, "y": <float>}

Physical-system parameter optimization.

You are optimizing physical system parameters.
 Goal: suggest k and b that minimize loss (smaller is better).
 Search bounds: k in [<k_min>, <k_max>], b in [<b_min>, <b_max>].
 Trial number: <trial_num>.
 Current best loss: <best_loss>.
 History of all previous attempts (step | k | b | loss):
 <history_lines>
 Important: do NOT repeat any previous (k, b) pair from history.
 Always propose new parameters that were not tried before.
 Return ONLY JSON in this exact format: {"k": <float>, "b": <float>}

BBOB function optimization.

You are optimizing an unknown black-box function (BBOB benchmark).
 Goal: suggest parameters that minimize this function.
 Search bounds: <bounds_str>.
 Trial number: <trial_num>.
 Current best loss: <best_loss>.
 History of all previous attempts (step | x0 | x1 | loss):
 <history_lines>
 Important: do NOT repeat any previous parameter combination.
 Always propose new parameters.
 Return ONLY JSON: <keys_desc>.

In the two-dimensional BBOB runs used in the main experiments, <bounds_str> has the form x0 in [<lower_0>, <upper_0>], x1 in [<lower_1>, <upper_1>], and <keys_desc> is {"x0": <float>, "x1": <float>}

D Evaluation Metrics for Pure BBO Optimization Problems

Each task τ fixes a bounded feasible region $\mathcal{X}_\tau \subset \mathbb{R}^d$ (e.g. $[0, 1]^2$ for the function family or the task-specific box for BBOB and parameter identification) that all four optimization settings see and must sample from. For each run we record the sequence of queried points $\{x_1, \dots, x_K\} \subset \mathcal{X}_\tau$ (with $K = 50$) and summarize behavior through three quantities.

Best step $\tau^* = \arg \min_{k \in \{1, \dots, K\}} y_k$ is the trial index at which the best loss is first attained, averaged over tasks. It measures how quickly an optimizer locks onto its final solution within the budget.

Coverage reports how broadly the domain has been probed. Let \bar{x}_k be the centroid of the first k queries and r_k the distance from \bar{x}_k to the farthest of them,

$$\bar{x}_k = \frac{1}{k} \sum_{i=1}^k x_i, \quad r_k = \max_{1 \leq i \leq k} \|x_i - \bar{x}_k\|_2. \quad (9)$$

Coverage is the area of the resulting bounding disk divided by the domain area,

$$\text{Cov}_k = \frac{\pi r_k^2}{S(\mathcal{X}_\tau)}. \quad (10)$$

Reported as a percentage, Cov_k indicates roughly how large a fraction of the search domain the optimizer has probed by step k .

Normalized trajectory length quantifies the straightness of the search path,

$$L = \frac{\|x_K - x_1\|_2}{\sum_{k=1}^{K-1} \|x_{k+1} - x_k\|_2} \in (0, 1]. \quad (11)$$

A perfectly linear trajectory attains $L = 1$. At the opposite extreme, an isotropic random walk with iid zero-mean increments of size s has total path length $(K-1)s$ and $\mathbb{E}\|x_K - x_1\|^2 = (K-1)s^2$, so its typical displacement scales as $s\sqrt{K}$ while its path length scales as Ks ; the ratio therefore obeys $L \approx 1/\sqrt{K}$, giving $L \approx 0.14$ at $K = 50$. High L means the optimizer moves mostly in one direction; low L means it jumps around.

E Greedy-Gradient Probe: Experimental Protocol

This section describes the experimental protocol underlying the greedy-gradient visualization in Figure 3. We detail the sampling procedure, the prompt setup, and the two prompt regimes (Table 3) used to verify that local refinement behavior is robust to prompt phrasing: across all four backbone-regime combinations, the model consistently anchors its proposals to the best observed point and steps toward the minimum in short local increments.

In each rollout, 10 points are sampled uniformly in $[0, 1]^2$ and evaluated. The full history is then passed to the LLM, which proposes 5 additional points (steps 11-15). The best of the first 10 points is highlighted in red in Figure 3 for visualization only; it is indistinguishable from the other nine in the prompt the model sees. The protocol is repeated for two backbones and two prompt regimes (Table 3). In all four conditions the geometry is the same: the LLM implicitly identifies the lowest-loss point, anchors its proposals to it, and steps toward the minimum in short local increments. The reasoning traces (Table 2 in the main text) confirm this: in every condition the model describes a gradient strategy to justify a local perturbation of the best seen point.

Black-box prompt	BO-style prompt
You are optimizing an unknown black-box function. Goal: suggest x and y that minimize this function (smaller is better). Search bounds: x and y must be in $[0, 1]$. Trial number: $\langle N \rangle$. Current best loss: $\langle \text{loss} \rangle$. History of all previous attempts (step x y loss): $\langle \text{history} \rangle$ Important: do NOT repeat any previous (x, y) pair from history. Return ONLY JSON in this exact format: $\{ "x": \langle \text{float} \rangle, "y": \langle \text{float} \rangle \}$.	You are optimizing an unknown black-box function. Goal: suggest x and y that minimize this function (smaller is better). Search bounds: x and y must be in $[0, 1]$. Trial number: $\langle N \rangle$. Current best loss: $\langle \text{loss} \rangle$. History of all previous attempts (step x y loss): $\langle \text{history} \rangle$ Important: do NOT repeat any previous (x, y) pair from history. Return ONLY JSON in this exact format: $\{ "x": \langle \text{float} \rangle, "y": \langle \text{float} \rangle \}$. Optimize like Bayesian optimization!

Table 3: The two prompt regimes used in Figure 3. The *BO-style* prompt appends a single line; everything else is identical.

F Prompt Templates for Shape-Conditioned Zero-Shot Generation

We use two closely matched prompt templates to test whether failures to condition on input shape are caused by the location of the size information in the prompt. In the *explicit* condition, the target dimensions appear in the reference context and are also repeated at the end of the prompt as a final instruction. In the *hidden-prompt* condition, the target dimensions remain only in the reference context, without the final explicit reminder. The hidden template can also omit the hypothesis requirement in single-shot mode through `require_hypothesis=not_is_single_shot`.

Explicit target-size prompt.

Your task is to implement an optimized version of the kernel provided in the `<reference>` section. Maximize the kernel's performance using various optimization strategies, ensure that the output remains numerically identical to the provided reference and avoid memory errors.

Strictly adhere to these requirements:

1. **Class Definition:** You must define a class named exactly `ModelNew`. This is the entry point used to instantiate your kernel.
2. **Inheritance:** The class must inherit from `torch.nn.Module`.
3. **Initialization:** `__init__(self, ...)` must accept the arguments provided by the reference implementation's `get_init_inputs()`.
4. **Forward Pass:** `forward(self, ...)` must accept the arguments provided by the reference implementation's `get_inputs()`.
- **Example:** If the baseline `get_inputs()` returns `[x, y]`, your method signature must be `forward(self, x, y)`.
5. **Output:** The return value of `forward` must have the exact same shape and data type as the reference output.
6. Use `torch.utils.cpp_extension.load_inline` to compile C++/CUDA source strings.
7. Do not write any code except described above.
8. Make code agnostic to device number, allocate output on the same GPU as the input (e.g. using `input.options()`).
9. Start code with `# Hypothesis: ... comment`.

```
{% if hardware_info %}
**Target Hardware:**
{{ hardware_info }}{% if compute_capability %} (Compute Capability: {{ compute_capability }}){% endif %}
{% endif %}
```

```
<reference>
{{ reference_code }}
</reference>
```

Start the file with a single comment line: `# Hypothesis: <your plan>` - briefly describe which specific optimization technique you are applying and why you expect it to improve{% if last_code %} (fix compilation, fix correctness, or increase speedup){% else %} performance{% endif %}.

```
{% if example_pre and example_after and not last_code %}
Refer to the following example to see how to rewrite a PyTorch model to an Inline CUDA model.
```

```
<example_pre>
{{ example_pre }}
</example_pre>
```

```
<example_after>
# Hypothesis: ...
{{ example_after }}
</example_after>
{% endif %}
```

```
{% if history %}
**Previous attempts (oldest first):**
{% for entry in history %}
- Hypothesis: {{ entry.hypothesis or '(none)' }}
Result: {% if not entry.result.compiled %}Compilation failed: {{ (entry.result.compilation_error or '') }}{% elif not entry.result.valid %}Incorrect: {{ (entry.result.correctness_info or '') }}{% if entry.result.speedup is not none %} (speedup: {{ "%.2f"|format(entry.result.speedup) }}){% endif %}{% elif entry.result.speedup is none %}Correct but performance measurement failed or timed out{{ (' ' ~ entry.result.performance_info) if entry.result.performance_info }}{% else %}Correct, speedup: {{ "%.2f"|format(entry.result.speedup) }}x{% endif %}
{% endfor %}
{% endif %}
```

```
{% if last_code %}
**Last attempt:**
<last_attempt>
{{ last_code }}
</last_attempt>
```

```
**Result:**
{% if not last_result.compiled %}
Compilation failed:
{{ (last_result.compilation_error or '') }}
{% elif not last_result.valid %}
Incorrect results:
{{ (last_result.correctness_info or '') }}
{% if last_result.speedup is not none %}
Performance: {{ "%.2f"|format(last_result.speedup) }}x
{% endif %}
{% elif last_result.speedup is none %}
Correct but performance measurement failed or timed out{{ (' ' ~ last_result.performance_info) if last_result.performance_info }}
{% else %}
Correct, speedup: {{ "%.2f"|format(last_result.speedup) }}x
{% endif %}
{% endif %}
```

Now write the new version of the kernel.

```
**IMPORTANT:** Begin your response with # Hypothesis: <your plan>.
```

```
{% if target_dims_text %}
**IMPORTANT (target sizes):** Optimize and validate the kernel specifically for these dimensions: {{ target_dims_text }}.
Treat these sizes as the primary optimization target.
{% endif %}
```

Implicit condition.

Your task is to implement an optimized version of the kernel provided in the `<reference>` section. Maximize the kernel's performance using various optimization strategies, ensure that the output remains numerically identical to the provided reference and avoid memory errors.

Strictly adhere to these requirements:

```
1. **Class Definition:** You must define a class named exactly ModelNew. This is the entry point used to instantiate your kernel.
2. **Inheritance:** The class must inherit from torch.nn.Module.
3. **Initialization:** __init__(self, ...) must accept the arguments provided by the reference implementation's get_init_inputs().
4. **Forward Pass:** forward(self, ...) must accept the arguments provided by the reference implementation's get_inputs().
   - *Example:* If the baseline get_inputs() returns [x, y], your method signature must be forward(self, x, y).
5. **Output:** The return value of forward must have the exact same shape and data type as the reference output.
6. Use torch.utils.cpp_extension.load_inline to compile C++/CUDA source strings.
7. Do not write any code except described above.
8. Make code agnostic to device number, allocate output on the same GPU as the input (e.g. using input.options()).
{% if require_hypothesis %}9. Start code with # Hypothesis: ... comment.{% endif %}

{% if hardware_info %}
**Target Hardware:**
{{ hardware_info }}{% if compute_capability %} (Compute Capability: {{ compute_capability }}){% endif %}
{% endif %}

<reference>
{{ reference_code }}
</reference>

{% if require_hypothesis %}
Start the file with a single comment line: `# Hypothesis: <your plan>` - briefly describe which specific optimization technique you are
applying and why you expect it to improve{% if last_code %} (fix compilation, fix correctness, or increase speedup){% else %} performance{%
endif %}.
{% endif %}

{% if example_pre and example_after and not last_code %}
Refer to the following example to see how to rewrite a PyTorch model to an Inline CUDA model.

<example_pre>
{{ example_pre }}
</example_pre>

<example_after>
# Hypothesis: ...
{{ example_after }}
</example_after>
{% endif %}

{% if history %}
**Previous attempts (oldest first):**
{% for entry in history %}
- Hypothesis: {{ entry.hypothesis or '(none)' }}
  Result: {% if not entry.result.compiled %}Compilation failed: {{ (entry.result.compilation_error or '') }}{% elif not entry.result.valid
 %}Incorrect: {{ (entry.result.correctness_info or '') }}{% if entry.result.speedup is not none %} (speedup: {{
  "%.2f"|format(entry.result.speedup) }}x){% endif %}{% elif entry.result.speedup is none %}Correct but performance measurement failed or
  timed out{{ (': ' ~ entry.result.performance_info) if entry.result.performance_info }}{% else %}Correct, speedup: {{
  "%.2f"|format(entry.result.speedup) }}x{% endif %}

{% endfor %}
{% endif %}

{% if last_code %}
**Last attempt:**
<last_attempt>
{{ last_code }}
</last_attempt>

**Result:**
{% if not last_result.compiled %}
Compilation failed:
{{ (last_result.compilation_error or '') }}
{% elif not last_result.valid %}
Incorrect results:
{{ (last_result.correctness_info or '') }}
{% if last_result.speedup is not none %}
Performance: {{ "%.2f"|format(last_result.speedup) }}x
{% endif %}
{% elif last_result.speedup is none %}
Correct but performance measurement failed or timed out{{ (': ' ~ last_result.performance_info) if last_result.performance_info }}
{% else %}
Correct, speedup: {{ "%.2f"|format(last_result.speedup) }}x
{% endif %}
{% endif %}

Now write the new version of the kernel.

{% if require_hypothesis %}
**IMPORTANT:** Begin your response with `# Hypothesis: <your plan>`.
{% endif %}
```

G Dominant Zero-Shot Parameter Modes (Tabular Summary)

The table below matches the bar charts in Figure 4 (main text): each entry is the fraction of generations that fix the listed literal hyperparameter value, aggregated over the full shape grid and averaged over two experimental conditions—one in which the prompt explicitly states the tensor shape (*explicit*) and one in which no

size information is provided (*implicit*). Both conditions yield identical mode frequencies, so only the aggregate is shown.

The parameters are: **threads** - number of GPU threads per thread block; **BLOCK_SIZE** - number of input elements processed by one block; **shared_shape** - width of the shared-memory tile used in reductions; **TILE_K**, **TILE_M**, **TILE_N** - tile sizes along the K , M , and N loop-nest dimensions of the tiled matrix multiply.

Task	Parameter mode	$T = 0.1$	$T = 0.5$	$T = 0.8$
Softmax	threads=256	36.0%	41.5%	43.5%
Softmax	BLOCK_SIZE=256	36.5%	38.5%	37.5%
Softmax	shared_shape=256	6.5%	9.0%	11.5%
Matmul with A^T	TILE_K=32	27.5%	27.5%	25.5%
Matmul with A^T	TILE_M=32	27.0%	26.5%	25.5%
Matmul with A^T	TILE_N=32	27.0%	26.5%	25.5%
Fused conv kernel	threads=256	82.0%	79.0%	79.5%
Fused conv kernel	BLOCK_SIZE=256	10.5%	10.5%	11.5%

Table 4: Dominant zero-shot parameter modes across temperatures. Each value is the fraction of generations using the listed parameter value, aggregated over the full shape grid (explicit and implicit shape-prompt conditions combined). The same few modes dominate at all sizes and temperatures, confirming that generation is governed by a fixed prior rather than by size-conditioned exploration.

H Unscheduled TVM-TIR Reference Construction

Each TVM IR experiment starts from an *unscheduled* TensorIR module that captures the computation graph of the KernelBench task without any loop schedule, tiling, or parallelism annotations. The module is produced by the following fixed pipeline applied to the original PyTorch reference.

Step 1: PyTorch \rightarrow ONNX. The PyTorch Model class from each KernelBench task is traced and exported to ONNX via `torch.onnx.export`. When symbolic tracing fails (e.g. for models with data-dependent control flow), the pipeline falls back to `torch.fx.symbolic_trace` and converts directly to TVM Relax IR.

Step 2: ONNX \rightarrow TVM Relax IR. The ONNX model is ingested by TVM’s Relax ONNX frontend (`tvm.relax.frontend.onnx.from_onnx`) with all tensor shapes fixed to the evaluation inputs of the task, producing a high-level Relax IRModule.

Step 3: Relax lowering to TIR. A deterministic sequence of seven Relax compiler passes is applied in order: **LegalizeOps** (lower composite ops to TVM primitives), **FoldConstant**, **CanonicalizeBindings**, **Normalize**, **FuseOps** (operator fusion), **FuseTIR** (lower fused operator groups to `PrimFunc` blocks in TensorIR), and **DeadCodeElimination**. After **FuseTIR**, every computational kernel is represented as a `T.prim_func` with explicit loop nests over the output tensor axes, but with no schedule annotations: no loop splitting, no thread/block binding, no vectorization, no shared-memory staging. The resulting module is what we call the *unscheduled TVM-TIR reference*.

What the LLM and MetaSchedule receive. Both the LLM agent and TVM MetaSchedule start from the same unscheduled module. MetaSchedule applies its tuning search within an explicitly parameterised schedule space; the LLM agent receives the module serialised as a `TVMScript` string (via `IRModule.script()`) and is asked to return a rewritten version with schedule transformations applied. This ensures that both baselines begin from the same computational representation and that any performance difference is attributable solely to the scheduling strategy, not to front-end conversion choices.

I Benchmark Input-Size Variants

Table 5 lists the tensor shapes used in the benchmark-native and small-input regimes for all tasks in our study. Notation: M , N - output matrix dimensions (rows and columns); K - shared inner dimension of a matrix product; $batch$ - batch size; dim - feature or reduction dimension; C_{in} , C_{out} - input and output channel counts of a convolution; H , W - spatial height and width; k - convolution kernel size; in , $hidden$, out - input, hidden, and output feature dimensions of a linear layer.

J Agentic Pipeline Diagrams

Figure 9 illustrates the pipeline of each agentic architecture from two complementary perspectives: a flowchart view and a graph-structure view. Table 6 summarizes the key properties of both architectures.

K Full Feedback-Iteration Breakdown

Figure 10 expands Figure 7 from the first and last feedback iterations to the complete five-step trajectory.

Level	Task	Benchmark-native	Small-input
L1	Standard matmul	$M = 2048$ $K = 8192$ $N = 4096$	$M = 128$ $K = 512$ $N = 256$
L1	Softmax	batch = 4096 dim = 393216	batch = 4 dim = 384
L2	Conv2D + ReLU + bias add	batch = 128 $C_{in} = 64$ $C_{out} = 128$ $H = W = 128$ $k = 3$	batch = 32 $C_{in} = 16$ $C_{out} = 32$ $H = W = 32$ $k = 1$
L2	Gemm + Sigmoid + LSE	batch = 16384 in = 2048 hidden = 4096 out = 1024	batch = 512 in = 64 hidden = 128 out = 32
L2	Gemm + Swish + Divide + clamp stack	batch = 1024 in = 8192 out = 8192	batch = 64 in = 512 out = 512

Table 5: Tensor shapes for all tasks in the benchmark-native and small-input regimes. Values are taken directly from the matched `level1/level1-small` and `level2/level2-small` task definitions; task labels are shortened for readability. Variable notation is defined in the text above.

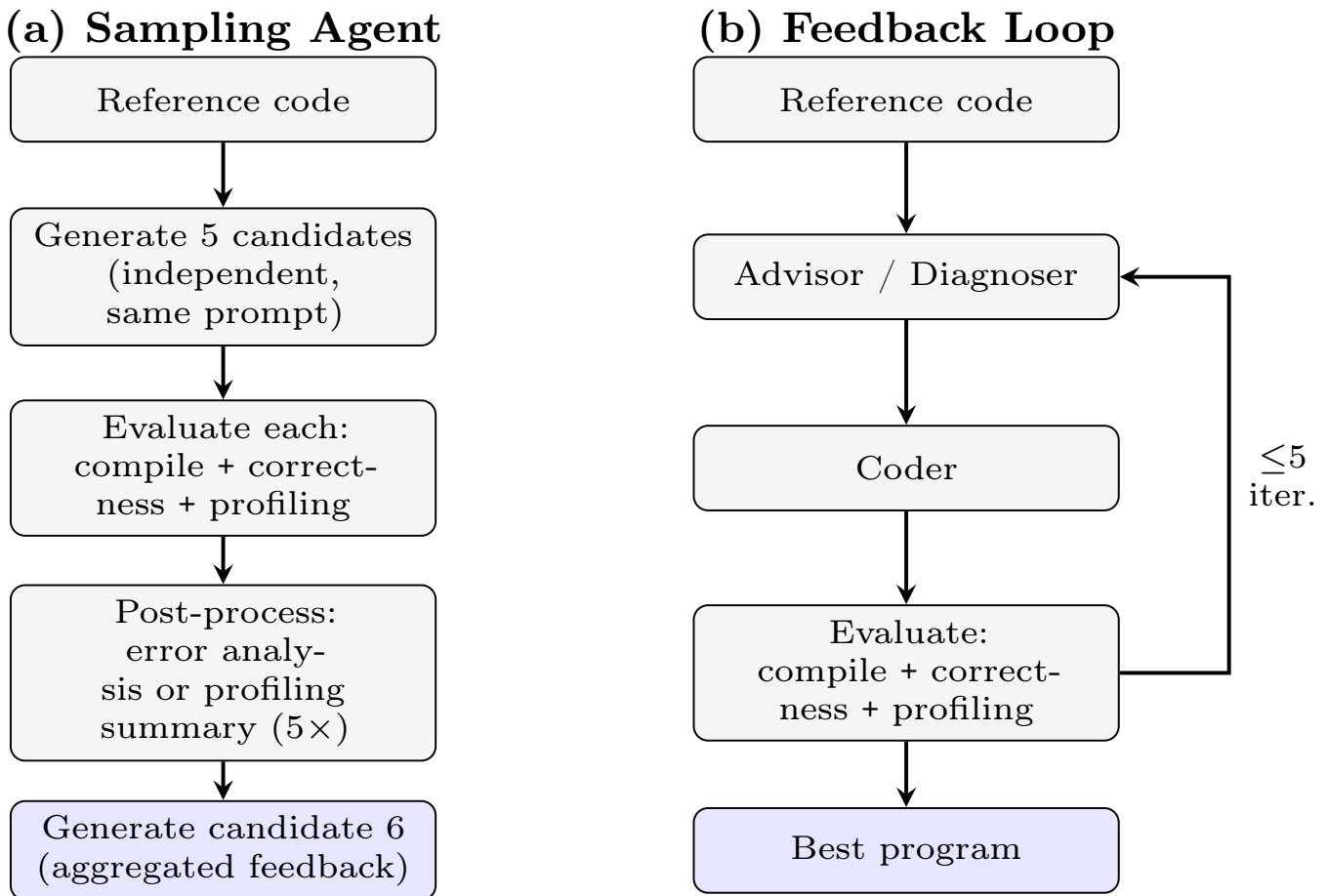


Figure 9: Pipeline diagrams for the two agentic architectures. **(a) Sampling Agent:** five candidates are generated independently from the reference and evaluated; post-processing converts each outcome into structured feedback, which is aggregated to generate a sixth candidate. **(b) Feedback Loop:** an advisor (on success) or diagnoser (on failure) iteratively steers a coder stage; up to five iterations, with the original reference and current best always in context.

Table 6: Summary of the two agentic architectures used in Section 4.2. #LLM is the maximum number of model calls per task: Sampling Agent = 5 coder + 5 advisor/diagnoser + 1 coder; Feedback Loop = 5 coder + 5 advisor/diagnoser.

Agent	Representation	#LLM	Search strategy	Feedback per step
Sampling Agent	CUDA, TVM IR	11	Parallel sampling; 6th candidate conditioned on 5 aggregated feedbacks	Error analysis or profiling summary (5x)
Feedback Loop	CUDA, TVM IR	10	Sequential refinement; advisor or diagnoser selected by outcome	Advice, profiling, and best-so-far in context

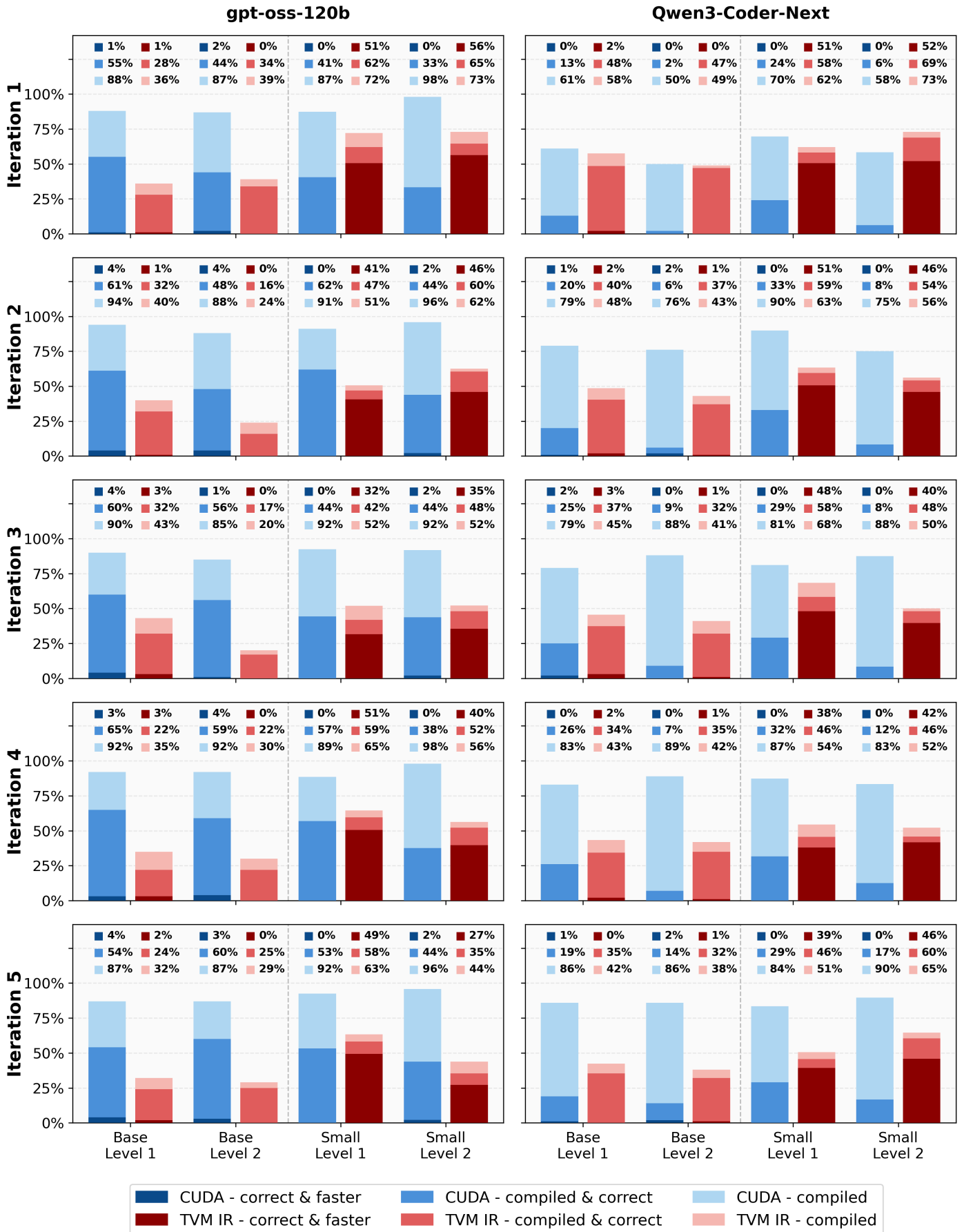


Figure 10: Expanded Feedback Loop validity and speedup under CUDA and TVM IR generation across all five feedback iterations. Bars use the same nested compile, correctness, and speedup encoding as the main-text figure.

L Additional TVM vs. torch.compile Size Sweeps

This appendix reports the full TVM MetaSchedule versus `torch.compile` size sweeps used to choose the stronger compiler baseline in the main text (Figures 11-15). The key takeaway is that TVM is faster in the small-input regime, which is why we use it as the primary non-LLM comparison there; as the problem size increases, the ranking becomes mixed and then partially reverses in favor of `torch.compile`. In every panel, the x-axis is the swept value of h .

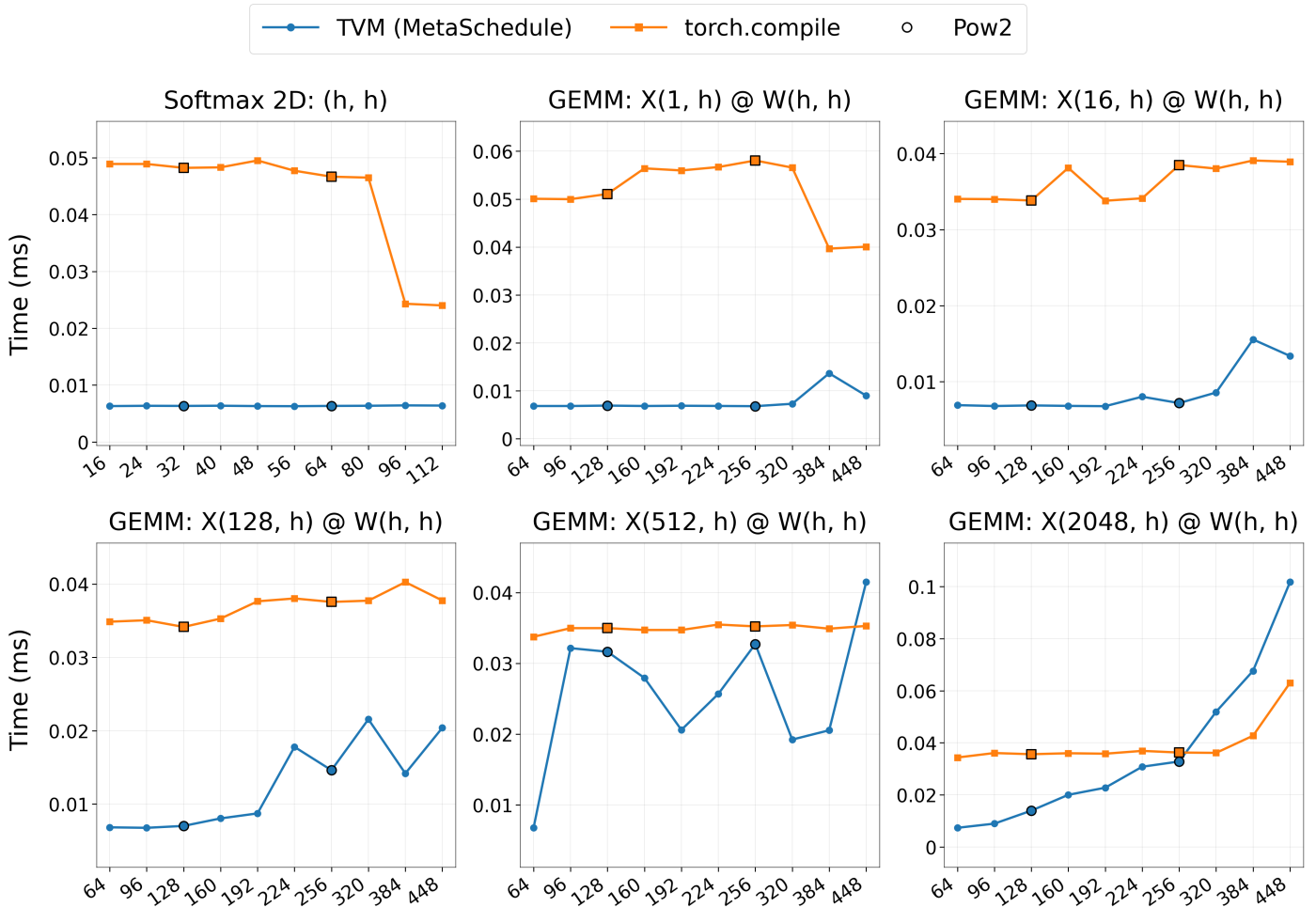


Figure 11: Extra-small size sweeps comparing TVM MetaSchedule and `torch.compile`. This is the clearest regime in which TVM dominates.

M Additional BBOB Optimization Traces

Figures 16-32 reproduce the seven-panel comparison layout used in the main text (Figure 1) for each task whose trace plot is stored under `media/bbob/`. Filenames match BBOB task identifiers (`bbob_fXX_..._iY`).

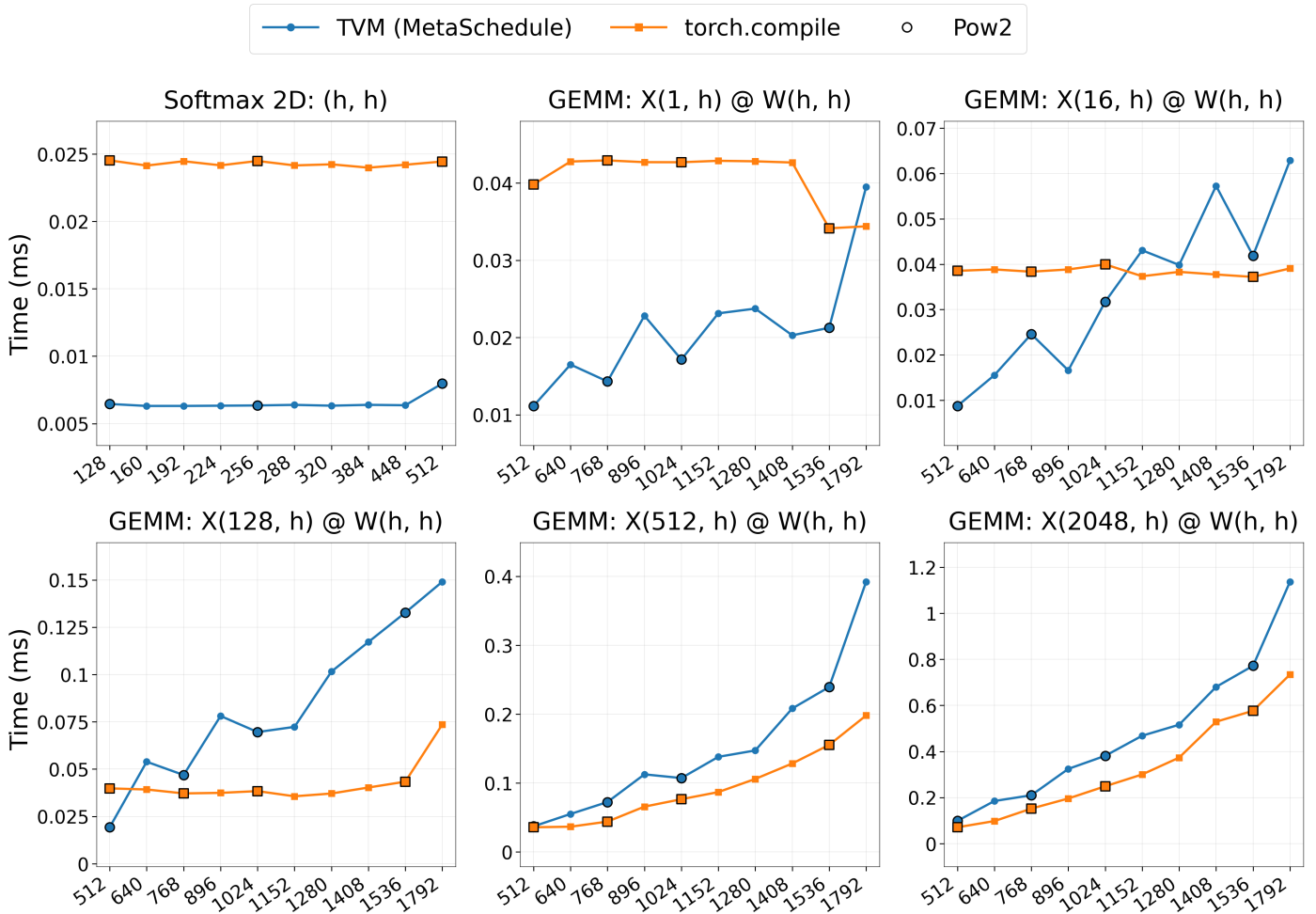


Figure 12: Small-size sweeps comparing TVM MetaSchedule and torch.compile. TVM remains stronger on most workloads in this regime.

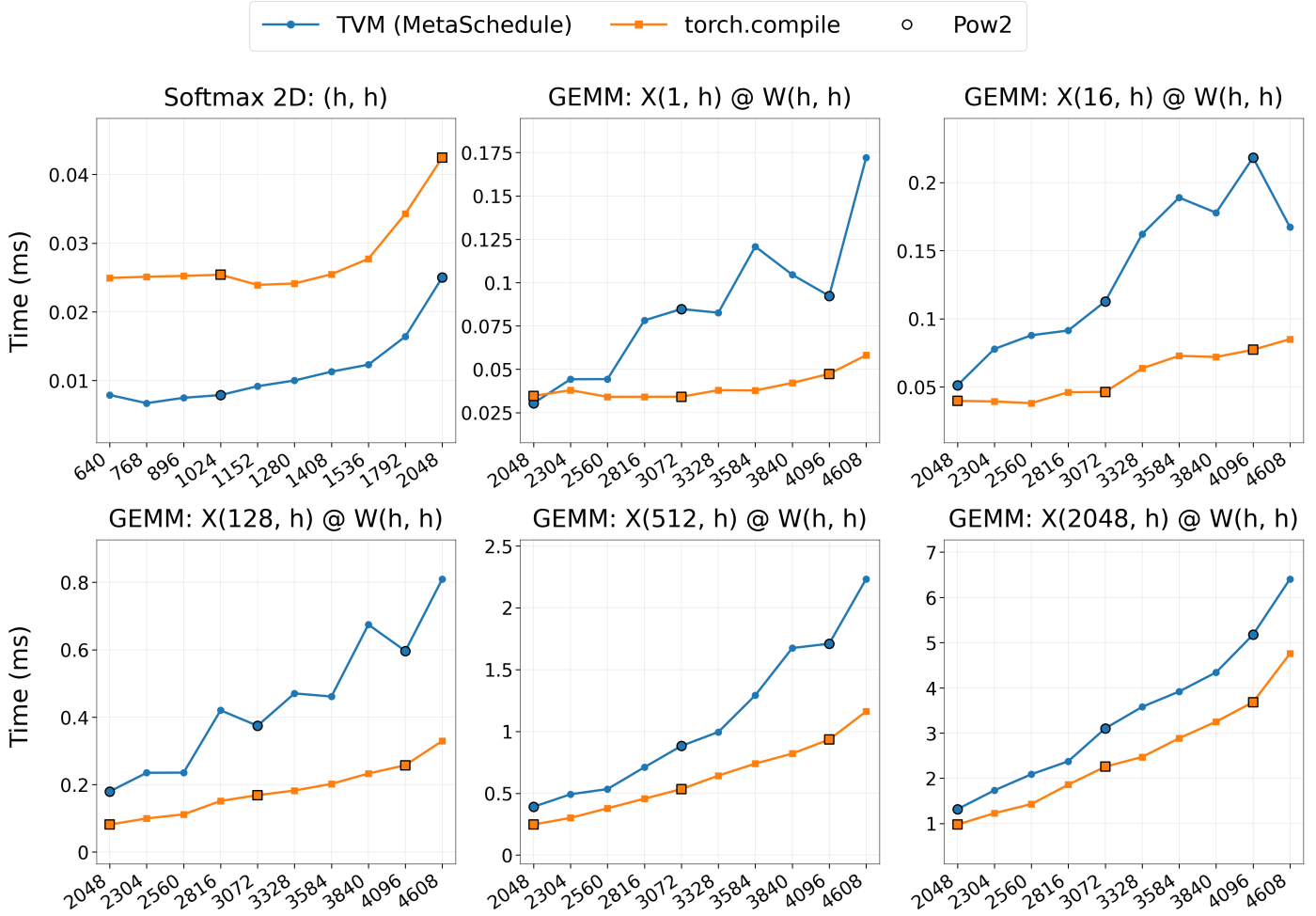


Figure 13: Medium-size sweeps comparing TVM MetaSchedule and torch.compile. The ranking becomes more mixed than in the small-input regime, indicating the onset of a regime transition.

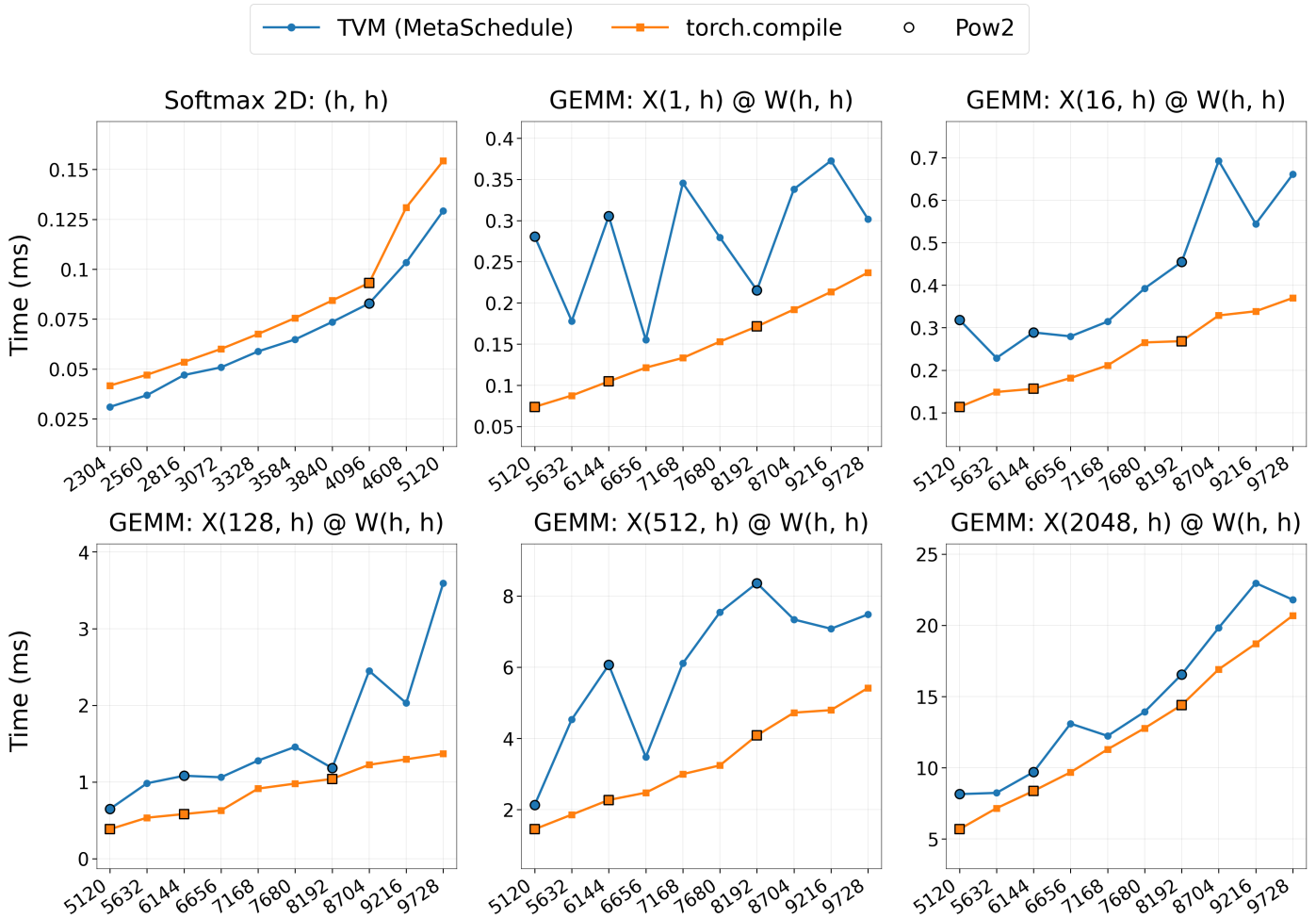


Figure 14: Large-size sweeps comparing TVM MetaSchedule and torch.compile. Relative performance is workload-dependent, and the torch.compile advantage becomes more visible than at small sizes.

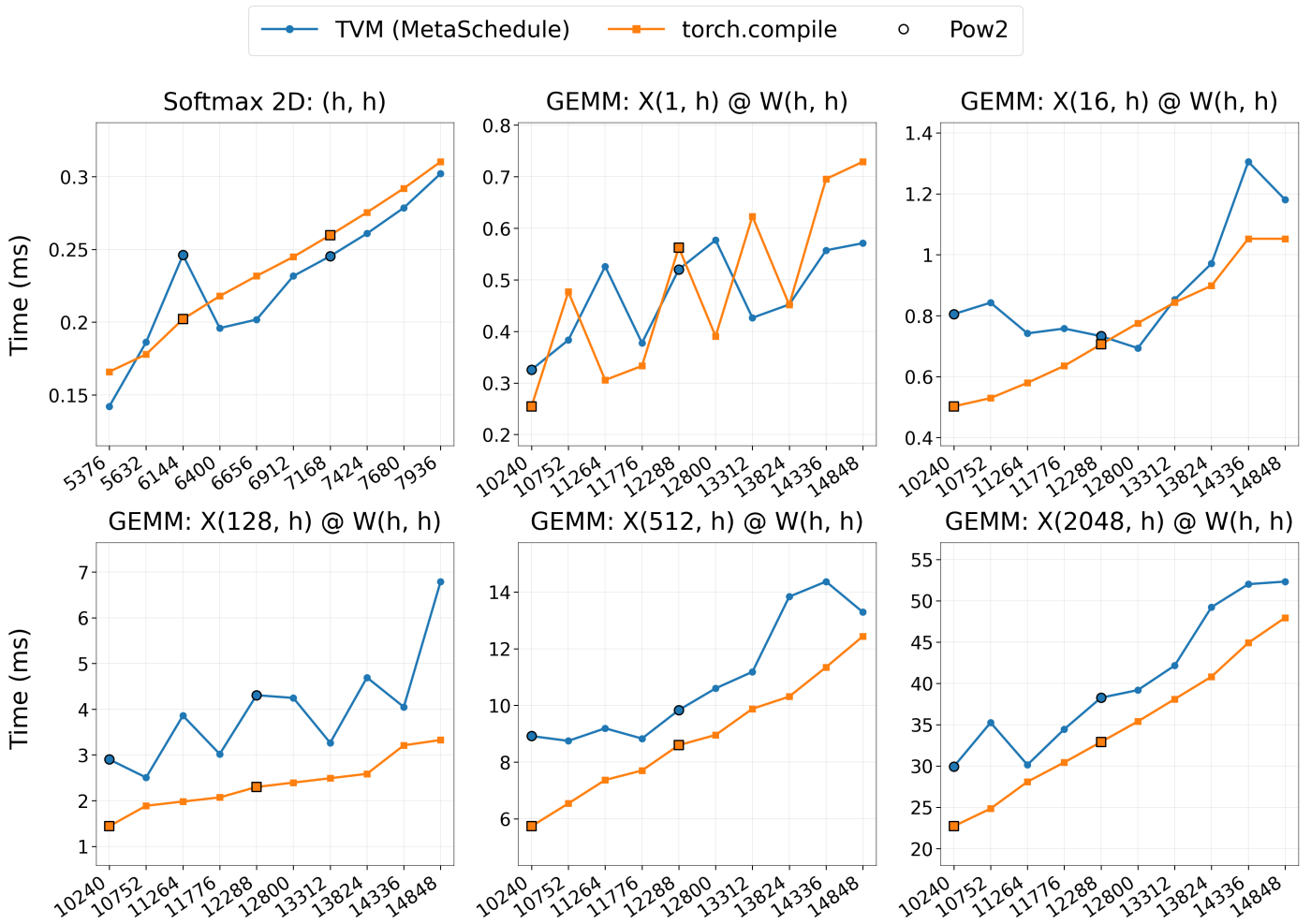


Figure 15: Extra-large size sweeps comparing TVM MetaSchedule and torch.compile. This regime most clearly shows the recovery of torch.compile at larger sizes.

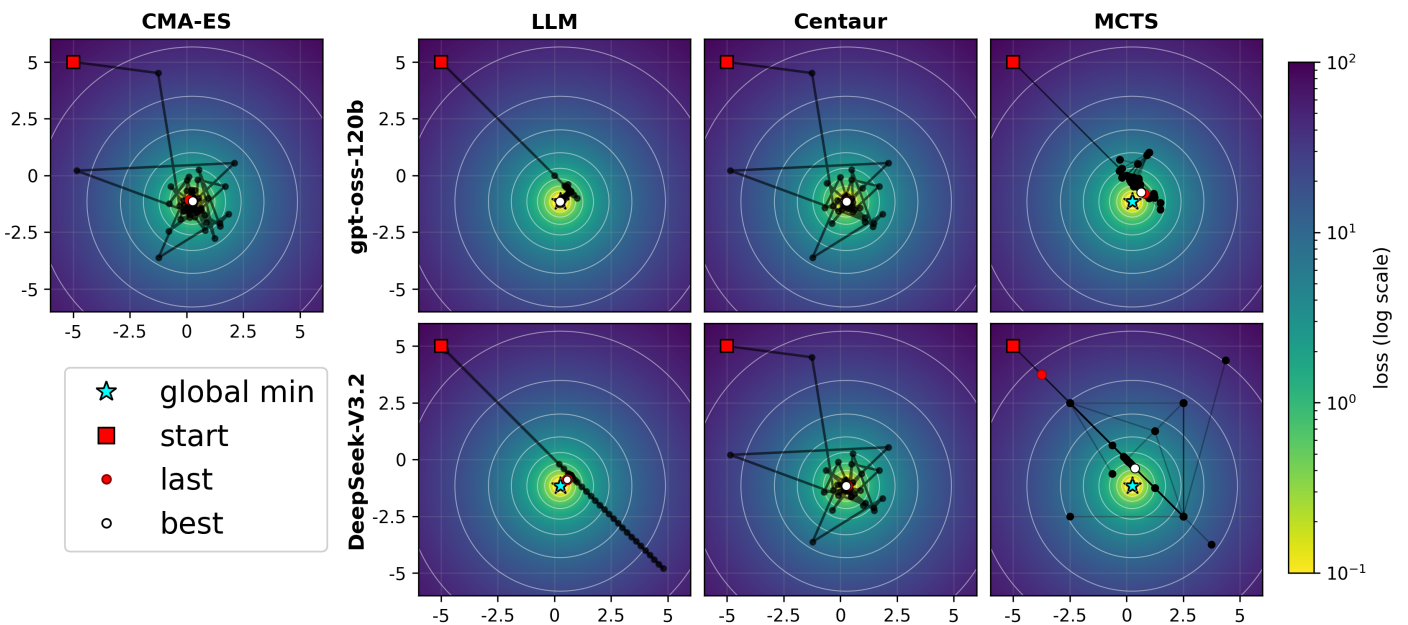


Figure 16: BBOB task bbob_f01_sphere_i1.

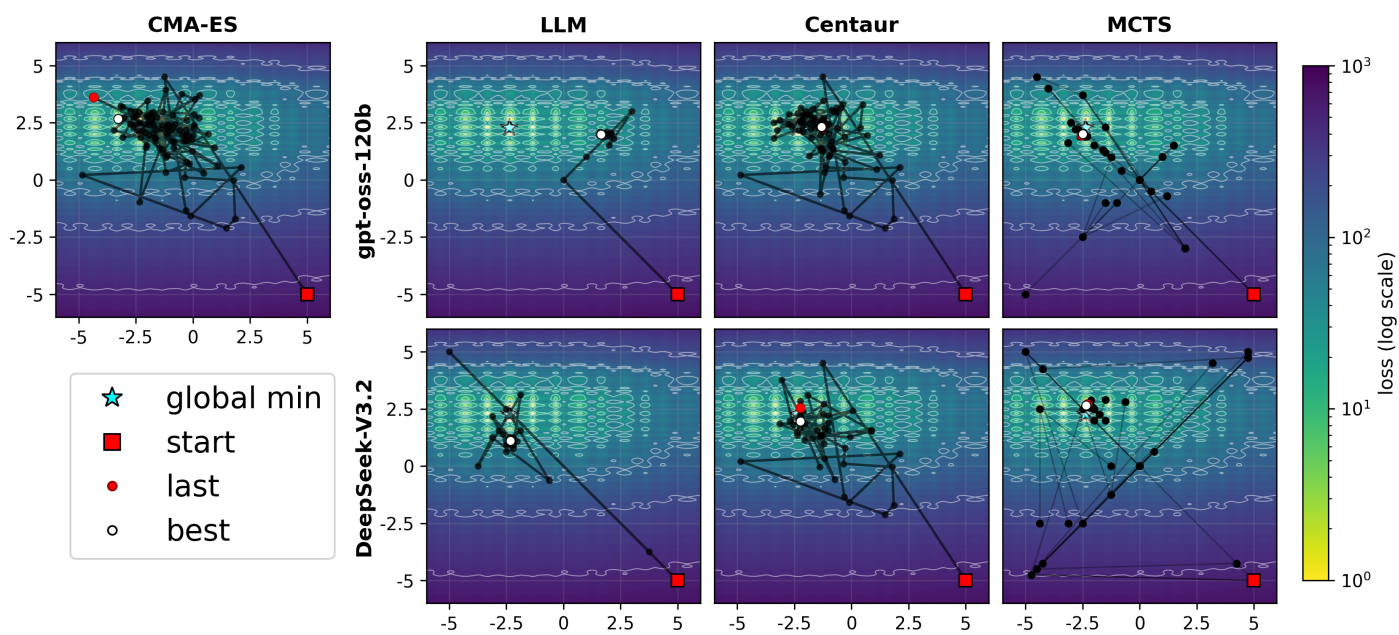


Figure 17: BBOB task `bbob_f03_rastrigin_i1`.

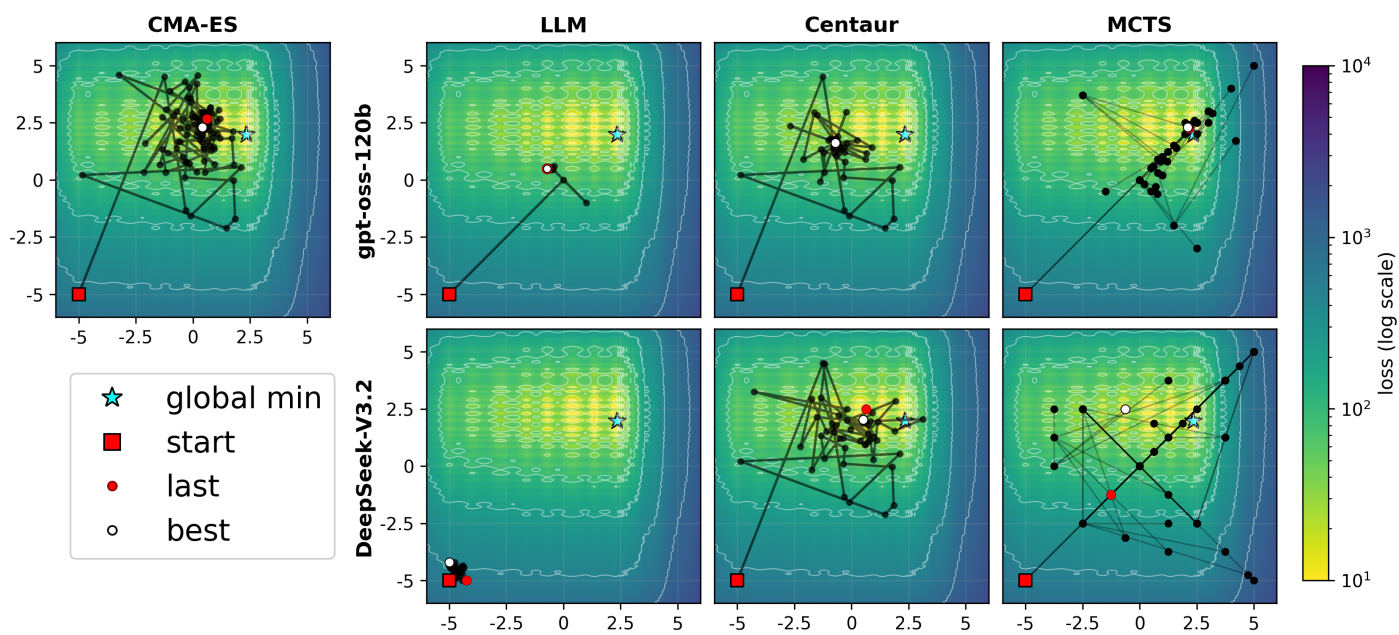


Figure 18: BBOB task `bbob_f04_bueche_rastrigin_i1`.

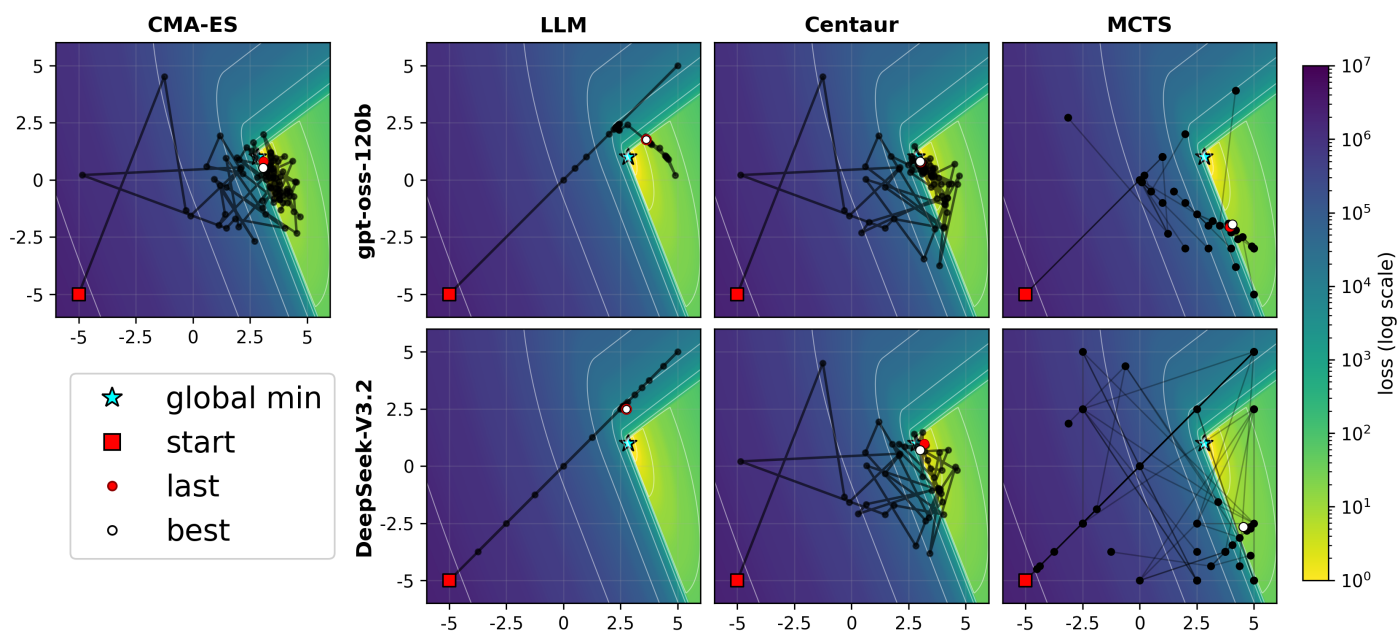


Figure 19: BBOB task `bbob_f06_attractive_sector_i1`.

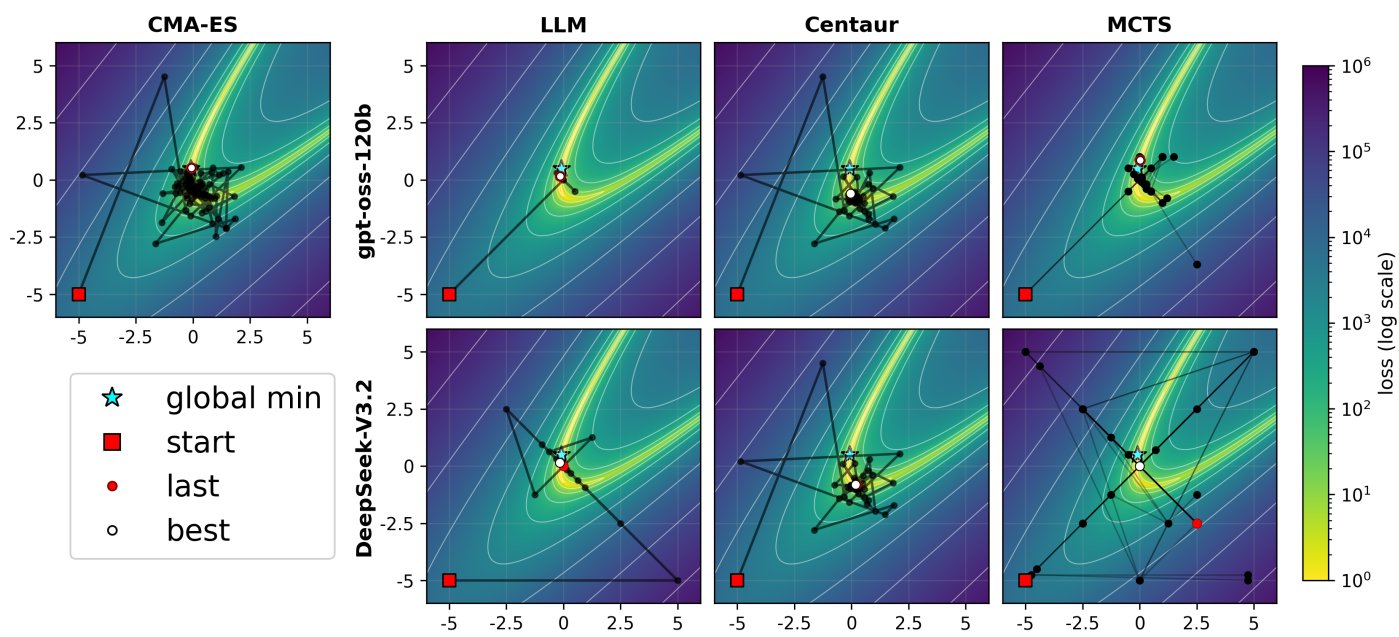


Figure 20: BBOB task `bbob_f09_rosenbrock_rotated_i1`.

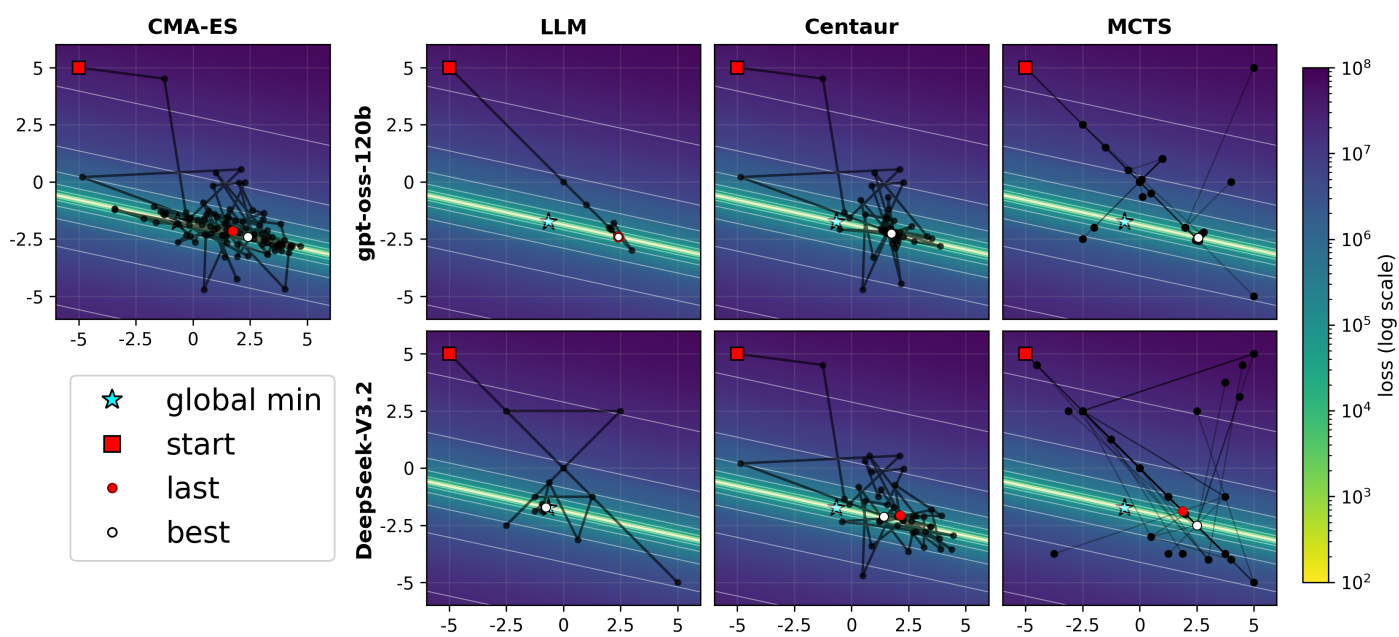


Figure 21: BBOB task `bbob_f10_ellipsoid_rotated_i1`.

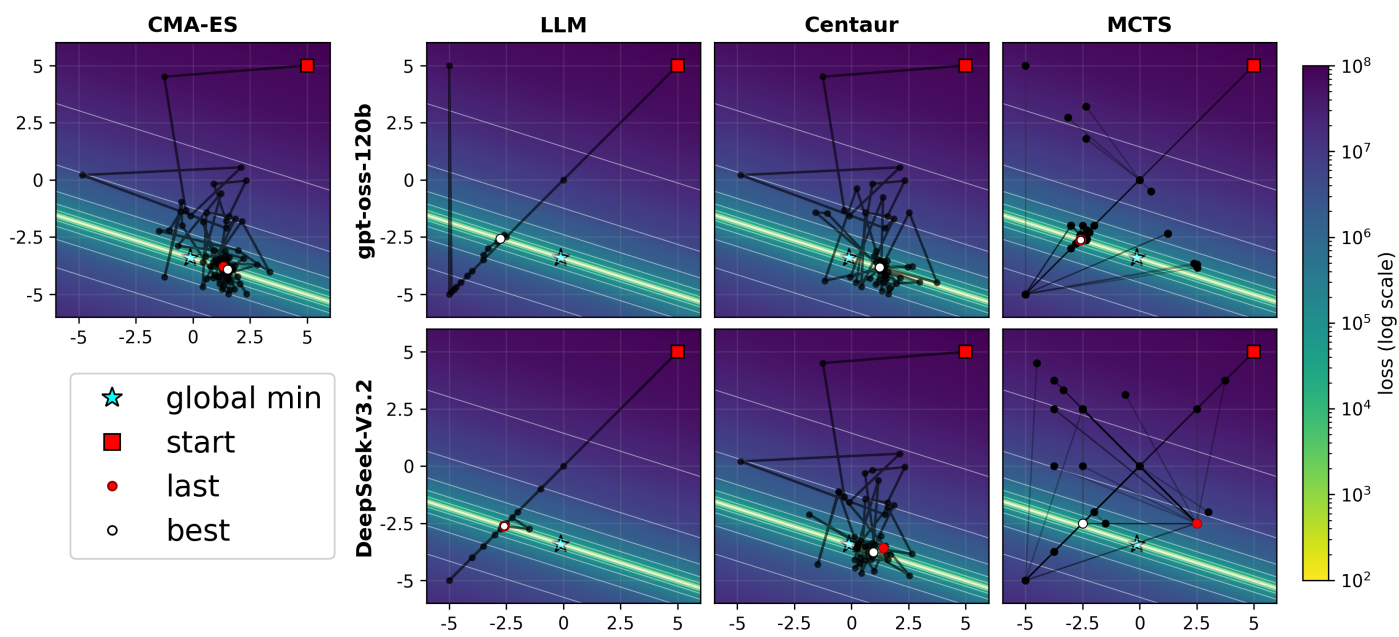


Figure 22: BBOB task `bbob_f11_discus_i1`.

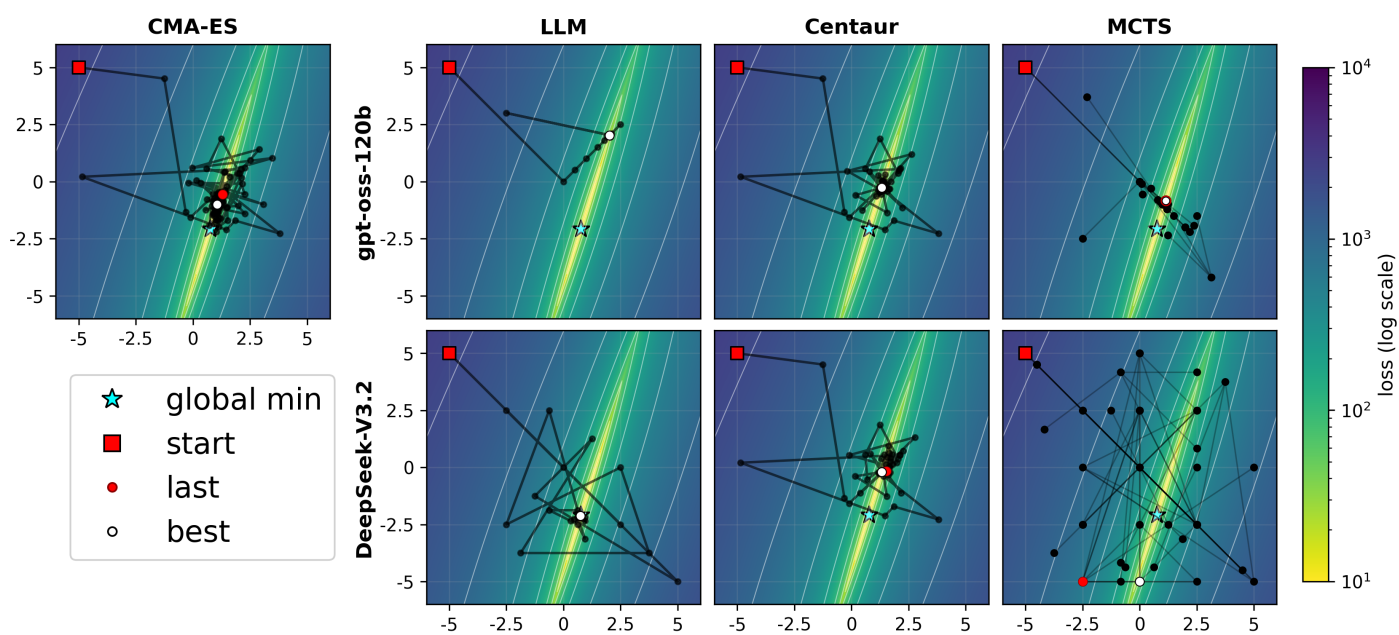


Figure 23: BBOB task `bbob_f13_sharp_ridge_i1`.

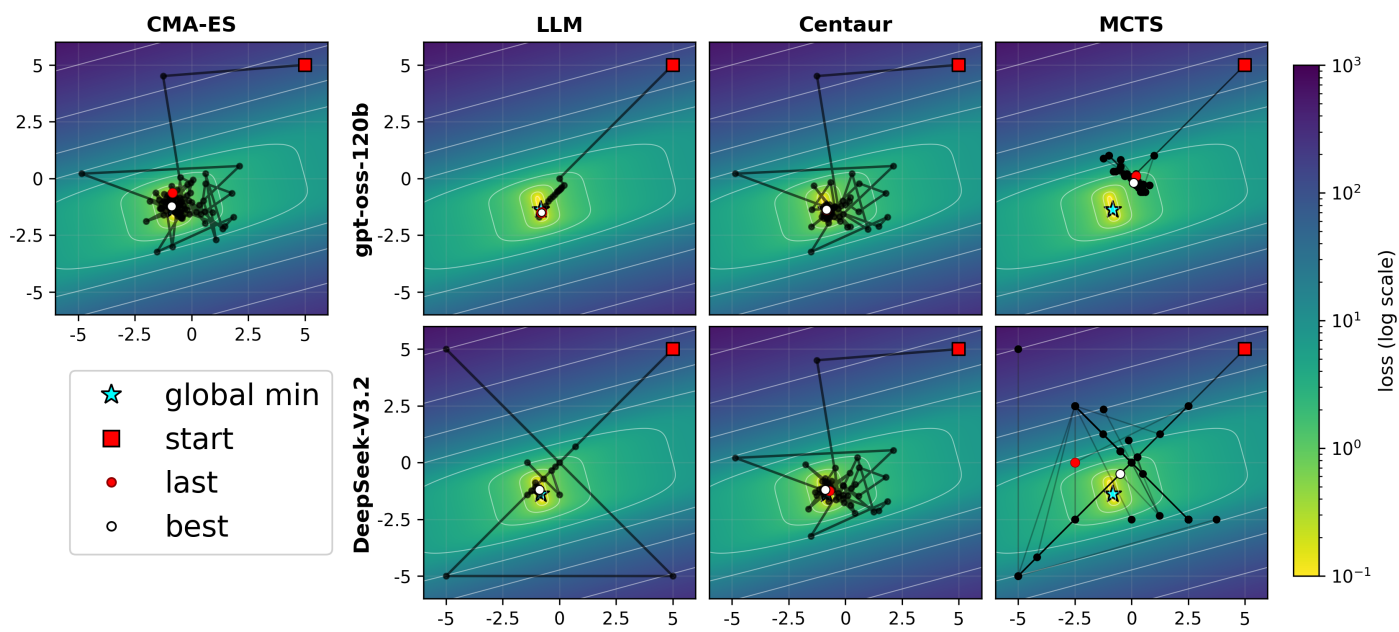


Figure 24: BBOB task `bbob_f14_different_powers_i1`.

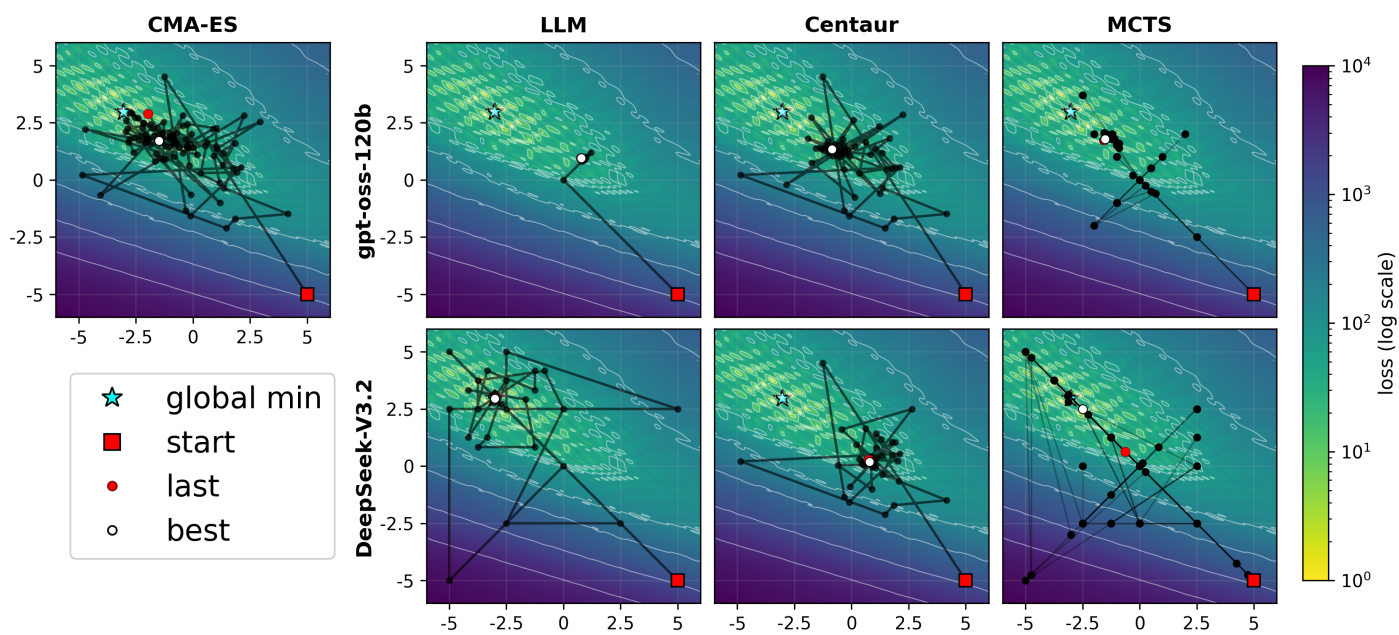


Figure 25: BBOB task `bbob_f15_rastrigin_rotated_i1`.

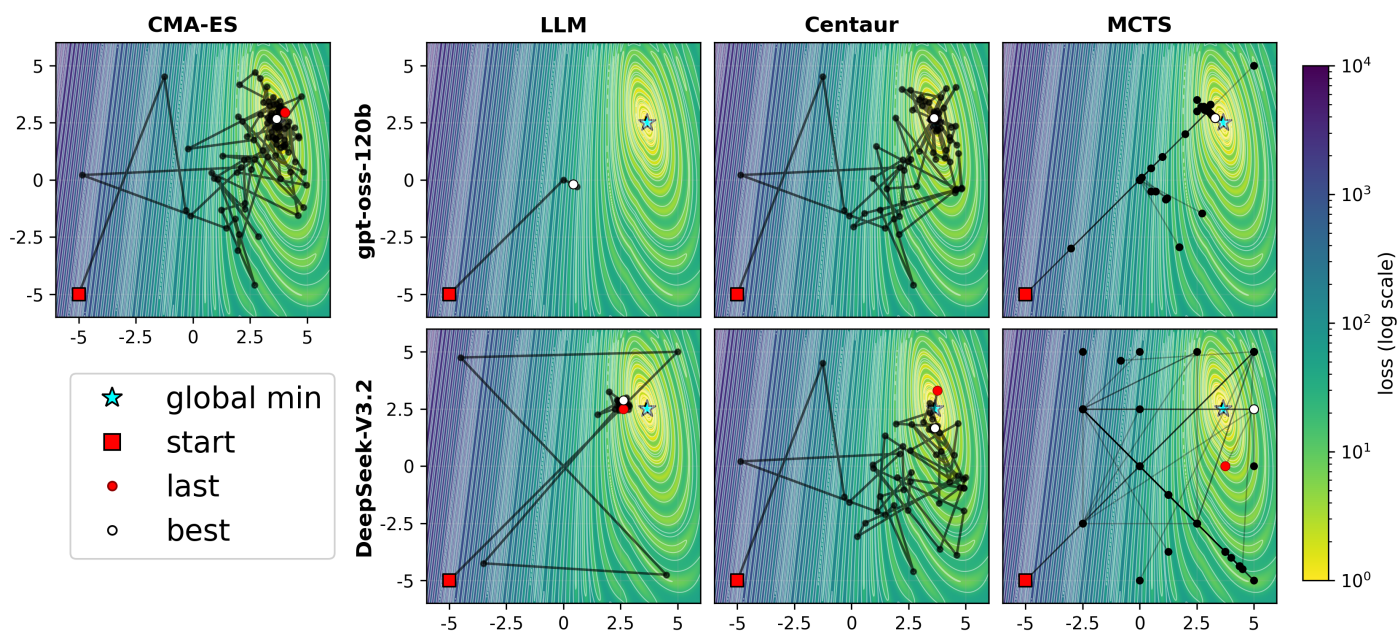


Figure 26: BBOB task `bbob_f17_schaffers_f7_i1`.

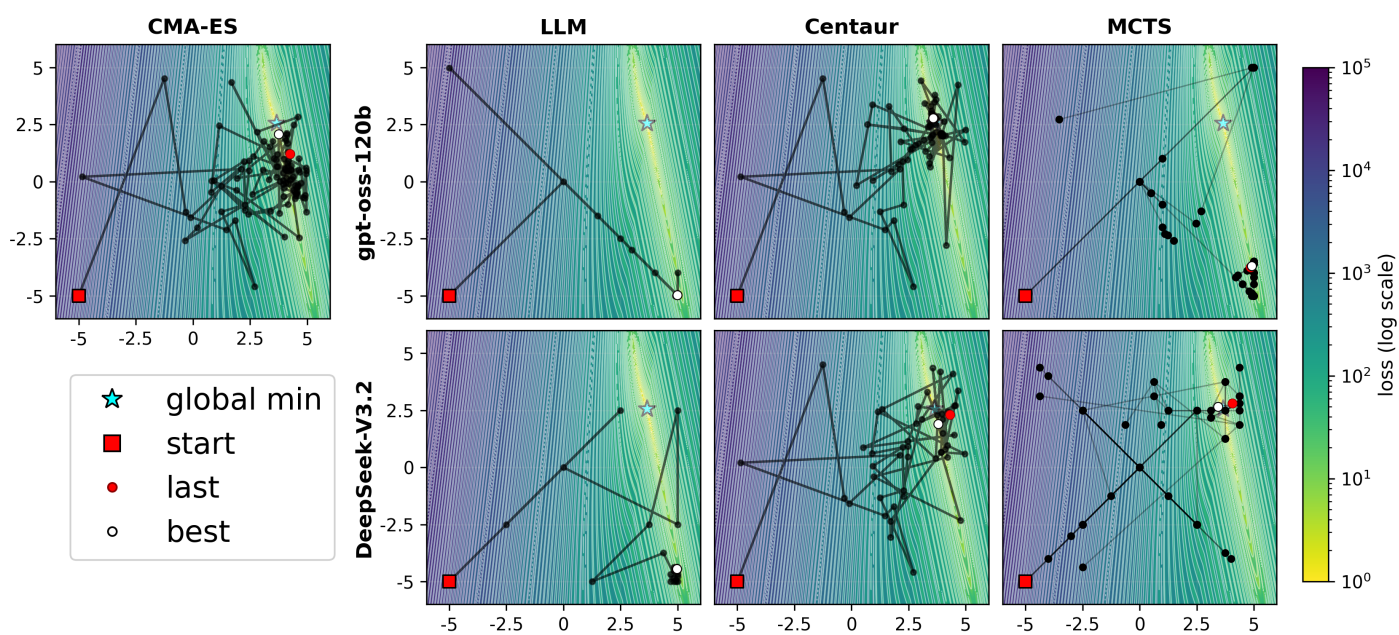


Figure 27: BBOB task `bbob_f18_schaffers_f7_ill_i1`.

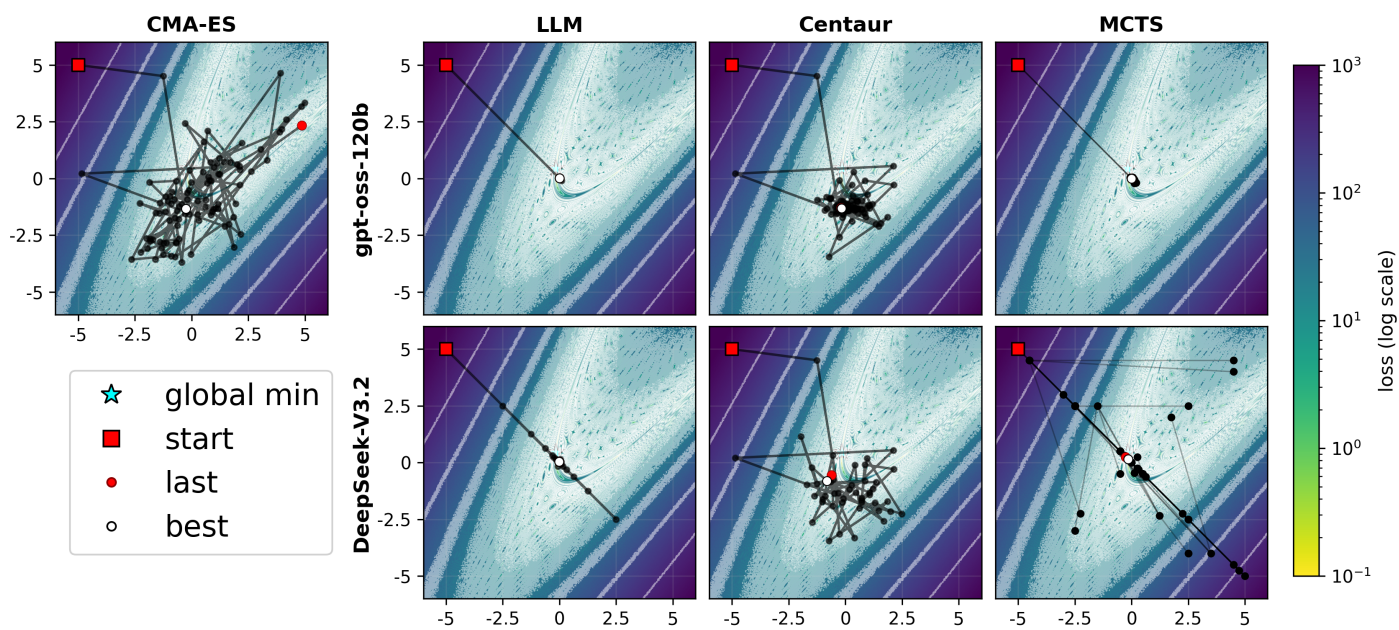


Figure 28: BBOB task `bbob_f19_griewank_rosenbrock_i1`.

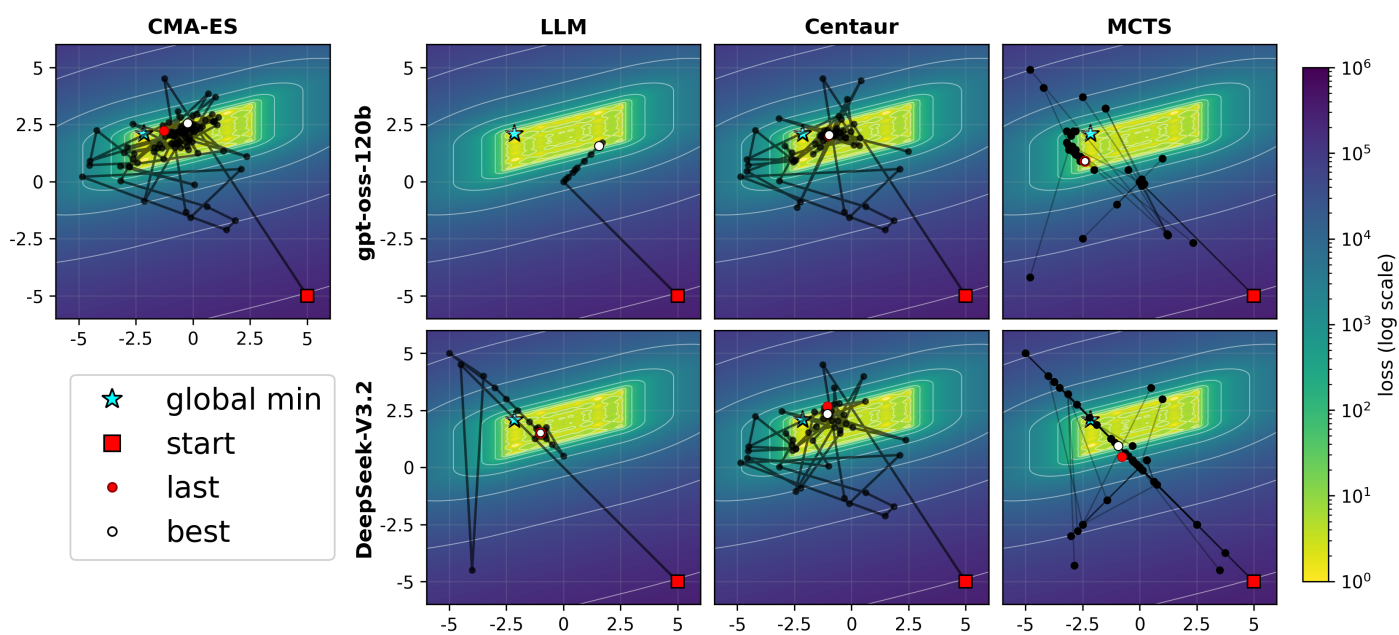


Figure 29: BBOB task `bbob_f20_schwefel_i1`.

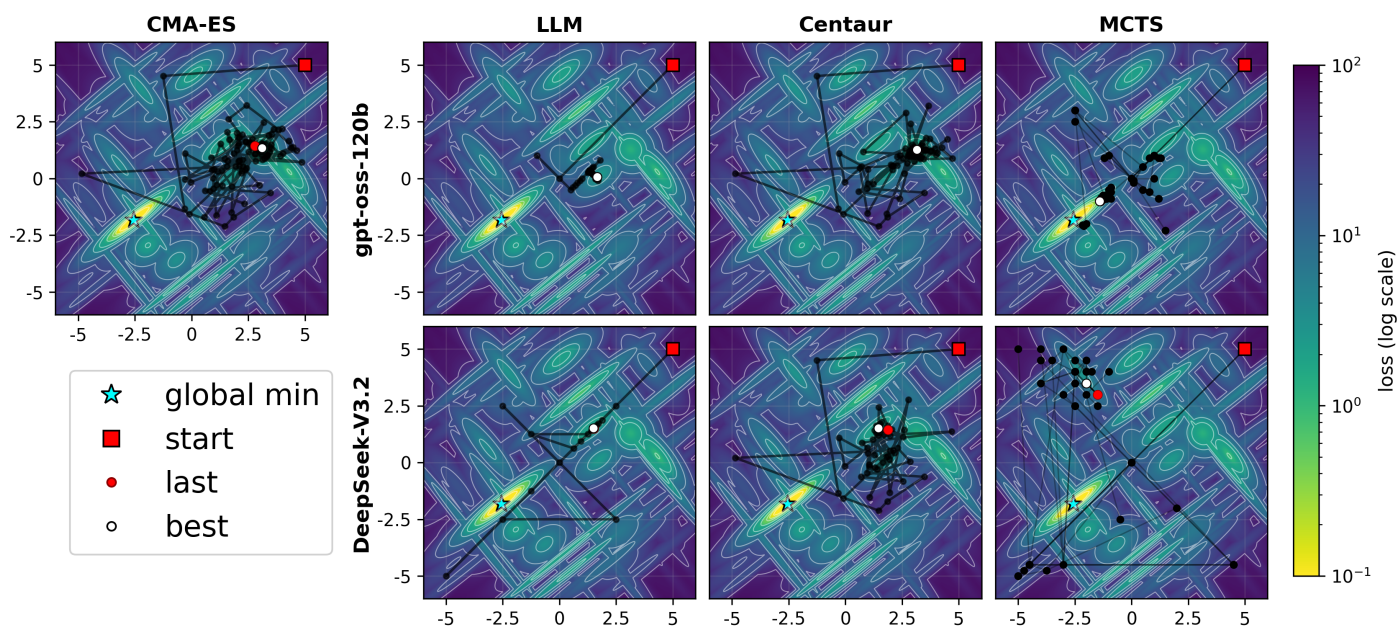


Figure 30: BBOB task `bbob_f21_gallagher_gaussian101_i1`.

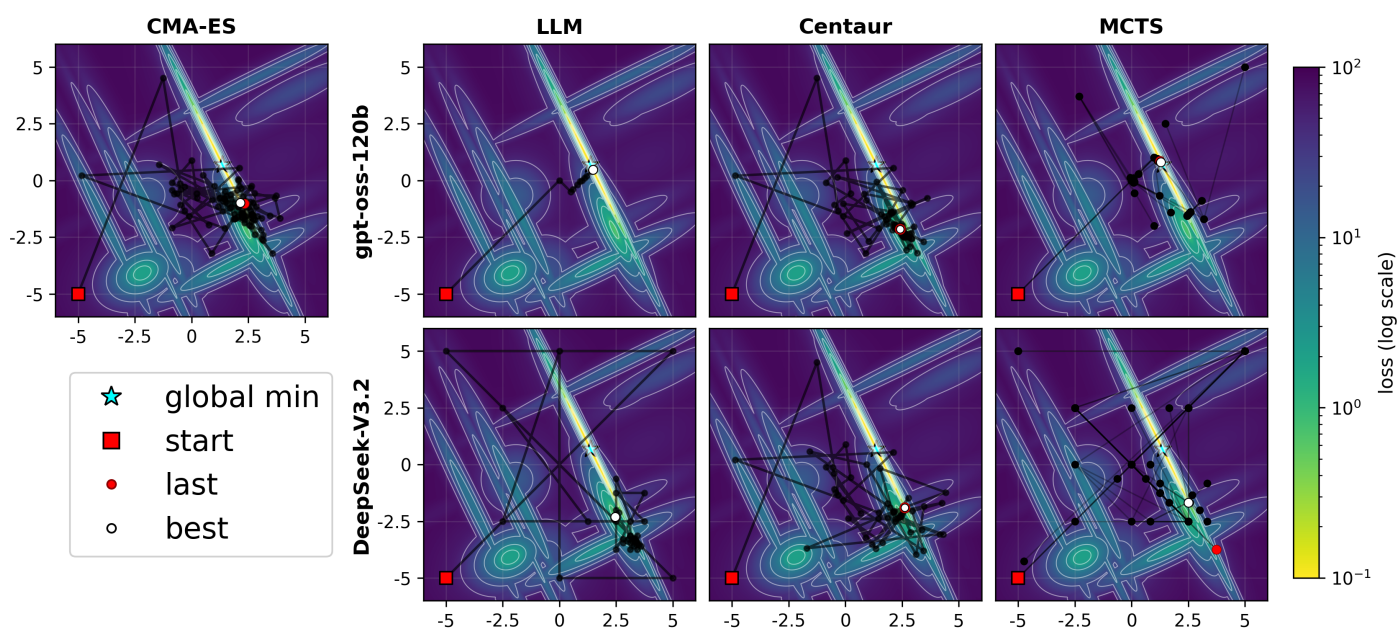


Figure 31: BBOB task `bbob_f22_gallagher_gaussian21_i1`.

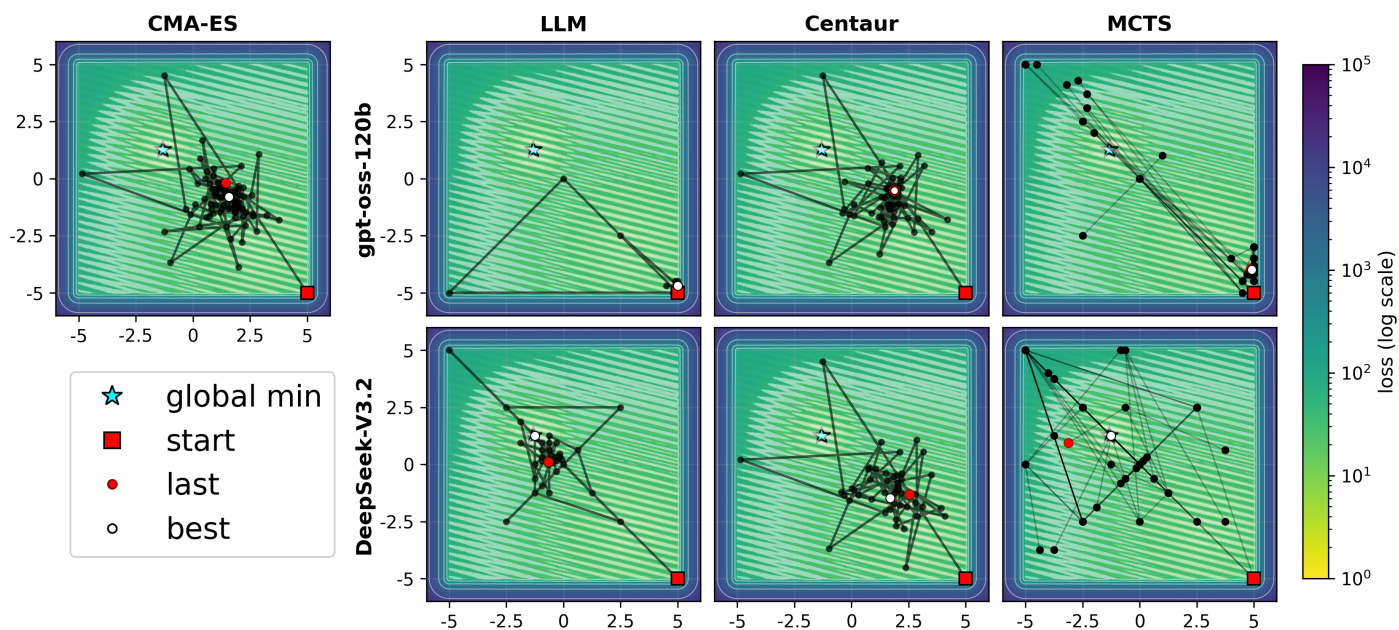


Figure 32: BBOB task `bbob_f24_lunacek_bi_rastrigin_i1`.